AWARD NUMBER: W81XWH-18-1-0542

TITLE: RET Kinase Signaling as a Key Switch Toward the Neuroendocrine Phenotype

PRINCIPAL INVESTIGATOR: Justin M. Drake and Leigh Ellis

CONTRACTING ORGANIZATION: University of Minnesota
Minneapolis, MN 55455

REPORT DATE: October 2020

TYPE OF REPORT: Annual

PREPARED FOR: U.S. Army Medical Research and Development Command
Fort Detrick, Maryland 21702-5012

REPORT DOCUMENTATION PAGE

Form Approved
OMB No. 0704-0188

1. REPORT DATE	2. REPORT TYPE	3. DATES COVERED
Oct 2020	Annual	09/30/2019-09/29/2020

4. TITLE AND SUBTITLE
RET Kinase Signaling as a Key Switch Toward the Neuroendocrine Phenotype

5a. CONTRACT NUMBER

5b. GRANT NUMBER
W81XWH-18-1-0542

5c. PROGRAM ELEMENT NUMBER

6. AUTHOR(S)
Justin M. Drake, Leigh Ellis

E-Mail:

5d. PROJECT NUMBER

5e. TASK NUMBER

5f. WORK UNIT NUMBER

7. PERFORMING ORGANIZATION NAME(S) AND ADDRESS(ES)
University of Minnesota
Minneapolis, MN 55455

Dana-Farber Cancer Institute
Boston, MA 02215-6013

8. PERFORMING ORGANIZATION REPORT NUMBER

9. SPONSORING / MONITORING AGENCY NAME(S) AND ADDRESS(ES)
U.S. Army Medical Research and Development Command
Fort Detrick, Maryland 21702-5012

10. SPONSOR/MONITOR'S ACRONYM(S)

11. SPONSOR/MONITOR'S REPORT NUMBER(S)

12. DISTRIBUTION / AVAILABILITY STATEMENT
Approved for Public Release; Distribution Unlimited

13. SUPPLEMENTARY NOTES

14. ABSTRACT
Increased treatment of metastatic castration resistant prostate cancer (mCRPC) with second-generation anti-androgen therapies (ADT) has coincided with a greater incidence of lethal, aggressive variant prostate cancer (AVPC) tumors that have lost androgen receptor (AR) signaling. AVPC tumors may also express neuroendocrine markers, termed neuroendocrine prostate cancer (NEPC). Recent evidence suggests kinase signaling may be an important driver of NEPC. To identify targetable kinases in NEPC, we performed global phosphoproteomics comparing AR-negative to AR-positive prostate cancer cell lines and identified multiple altered signaling pathways, including enrichment of RET kinase activity in the AR-negative cell lines. Clinical NEPC and NEPC patient derived xenografts displayed upregulated RET transcript and RET pathway activity. Pharmacologically inhibiting RET kinase in NEPC models dramatically reduced tumor growth and cell viability in mouse and human NEPC models. Our results suggest that targeting RET in NEPC tumors with high RET expression and may be a novel treatment option.

15. SUBJECT TERMS
RET kinase, castration resistant prostate cancer, aggressive variant prostate cancer, kinase inhibitors, mouse models, organoids

16. SECURITY CLASSIFICATION OF:			17. LIMITATION OF ABSTRACT	18. NUMBER OF PAGES	19a. NAME OF RESPONSIBLE PERSON
a. REPORT	b. ABSTRACT	c. THIS PAGE			USAMRMC
Unclassified	Unclassified	Unclassified	Unclassified	31	19b. TELEPHONE NUMBER *(include area code)*

TABLE OF CONTENTS

INTRODUCTION

Prostate cancer (PCa) is the most common male cancer in the United States. Blocking androgen synthesis or signaling through the androgen receptor (AR) is the first line treatment. However, prostate cancer inevitably develops castration resistant prostate cancer (CRPC) and an emerging subset (35%) of CRPC patients develop a highly aggressive tumor phenotype designated aggressive variant prostate cancer (AVPC) and treatment provides modest 1-2 years survival rates. AVPC is characterized by low to absent AR levels and expression of neuronal, reprogramming and stem related gene signatures. Previously, we observed tyrosine phosphorylation of RET, suggesting activity of this kinase in a patient with prostate AVPC. Our objectives are to 1.) Functionally assess the role of RET kinase in the transition to AVPC, 2.) Determine if RET kinase collaborates with EZH2 to drive AVPC, 3.) Determine RET dependent kinase signaling driving lineage plasticity, and 4.) Conduct preclinical trials to evaluate co-inhibition of RET kinase and EZH2 for treatment of AVPC, and re-sensitizing AVPC to enzalutamide. These all are important and unanswered questions involving the most lethal PCa phenotype observed clinically. Our success will drive the PCa field forward, and significantly alter clinical management of patients with AVPC.

KEYWORDS

Prostate Cancer; ADT; Castration Resistance; Enzalutamide; Lineage Plasticity, AVPC; NEPC; RET; Tyrosine Kinase, EZH2; Methylation; Epigenetics, Tyrosine Kinase Inhibitor, Organoids.

ACCOMPLISHMENTS

What were the major goals of the project?

Year 2 of this DOD application, the major goals for the Drake and Ellis lab were to:

Major Task #1:

1. Generate genetically engineered mice to stand as our breeding colony for generation of our planned experimental genotypes.

Major Task #2:

2. Assess the function of RET mutation on RET tyrosine phosphorylation in cell line models.

Major Task #4:

3. Begin the application for IRB approval to assess RET pathways on TMAs.

Major Task #5:

4. Assess novel RET inhibitors on cell line and organoid death.

Major Task #6:

5. We have published our work on RET kinase in AVPC models in *Mol Cancer Research*[1].

What was accomplished under these goals?

Major Task #1:

1. Generate genetically engineered mice to stand as our breeding colony for generation of our planned experimental genotypes. We had achieved our goal of generating 2x breeding colonies to generate experimental mice.

   Breeder Set 1: (Subtask 1) male mice with the genotype of PbCre:Pten$^{fl/fl}$:Rb1$^{fl/fl}$:Ret$^{fl/+}$ and female mice with the genotype Pten$^{fl/fl}$:Rb1$^{fl/fl}$:Ret$^{fl/fl}$.

   Breeder Set 2: (Subtask 2) male mice with the genotype of PbCre:Pten$^{fl/fl}$:Rb1$^{fl/fl}$:Ezh2$^{fl/+}$:Ret$^{fl/+}$ and female mice with the genotype Pten$^{fl/fl}$:Rb1$^{fl/fl}$:Ezh2$^{fl/fl}$:Ret$^{fl/fl}$.

We have been able to generate the desired genotypes from our proposal. It should be noted that we have encountered major complications in generating these mouse models, which have not been documented in the literature or at Jackson laboratories. The most common problems we have encountered/discovered are:

- Homozygote (RETlox/lox) mice demonstrate severe health problems independent of Cre recombinase expression. Mostly, we have observed that these mice die prematurely (<30 weeks of age).

- We observe a frequency of cystic kidneys within these mice and a minor phenotype observed is intestine obstruction (Fig. 1).
- We did not explore if these phenotypes are due to the fact that this model is engineered to express a human RET cDNA which may negatively affect any endogenous mouse Ret within this models.
- Another limiting phenotype we observed was decreased fertility in male mice which we attribute to atrophy of the testis.

Fortunately, we have a number of mice that we anticipate to successfully age to 28-30 weeks for each genotype. We anticipate that this will still allow us to conduct histopathology/IHC analysis, with enough tissue to also perform RNA sequencing to assess changes in gene expression due to loss or RET kinase expression and function. Because we have limited samples we propose to perform ATAC sequencing instead of our proposed ChIP sequencing. ATAC seq will still allow use to identify changes in chromatin remodeling due to loss or RET kinase expression and function. Table 1 highlights the numbers of mice we anticipate surviving to a 28-30 week endpoint. We have sacrificed and collected a total 15 mice of vary RET zygosity. The weights of these prostates is shown in Fig. 2. The remaining mice a due to be sacrificed over December 2020 – February 2021.

Table 1: Total number of mice with Pten:Rb1 double-out and differing RET zygosities for final analysis

	Alive	Harvested	total
Ret(+/+)	11	3	14
Ret(+/lox)	11	7	18
Ret(lox/lox)	2	4 (1)	7

As secondary models from our GEMMs we are generating 3-dimensional organoids and 2-dimensional cell lines. These lines will carry the matched alleles from the mouse models as assessed by standard genotyping PCR methods. An example of 3-dimensional organoid cultures can be seen in Fig. 3. Further, we are also using Pten:Rb1 double knock-out (DKO) mouse 2-dimensional cell lines and using CRISPR-Cas9 technology to KO Ret expression (Fig. 4). Our preliminary data indicates that our guide RNA targeting Ret kinase are specific and at least 2 (Ret1 and Ret 3) may provide adequate loss of Ret kinase to render them resistant to Ret Kinase chemical inhibition (Fig. 4).

Overall, this will provide various models to validate our upcoming experiments and potentially allow substitution if our final number of anticipated GEMM samples is inadequate.

Major Task #2:

2. We have begun creating RET mutants to assess RET activity in our cell line models. Overexpression of these mutants and wild type RET (Fig. 5A) can increase RET tyrosine phosphorylation in 293T cells (Fig. 5B). We are now investigating whether RET overexpression can alter RET phosphorylation in prostate cancer models.

Major Task #4:

3. We are in the process of applying for our human IRB protocol to assess RET-dependent pathways on clinical TMAs. We hope to stain those TMAs in 2021.

Major Task #5:

4. We have also tested new FDA approved RET inhibitors, BLU-667 and LOXO-292 on mouse organoid models of NEPC (Fig. 6A). Working with Dr. Ellis and using his double knockout (DKO) mouse model of $PTEN^{-/-}$ and $RB^{-/-}$, mimicking NEPC[2], we were able to show that the organoids grown from these DKO tumors showed a dose dependent effect to all of the RET inhibitors (Fig. 6A-D) and that NCI-H660 organoids were also sensitive to another RET inhibitor AD80 (Fig. 6E, F). We also and found that AD80 can synergize with enzalutamide (Fig. 7A, B), suggesting that RET inhibition may re-sensitize AR- tumors to enzalutamide (Subtask 2). We are investigating the mechanism as to how this may occur and testing several different combination therapies.

What opportunities for training and professional development has the project provided? The trainee, Dr. Yuzhen Zhou has successfully breeded the desired animals and begun collecting specimens with the Animal Resource Facility at Dana-Farber Cancer Institute. Dr. Halena VanDeusen in the Drake laboratory was able to attend the Society for Basic Urologic Research Annual Meeting and present her work on this project and has also published a first author manuscript from the work in the grant.

How were the results disseminated to communities of interest? To date, we have presented some aspects of our work to conferences including the Prostate Cancer Foundation Retreat and Society for Basic Urologic Research Annual Meeting in 2019 and 2020. We have also published this work to BioRxiv and the manuscript was accepted in *Molecular Cancer Research* in May 2020.

What do you plan to do during the next reporting period to accomplish the goals? We will continue our breeding of experimental mice (GEMMs) so that we can age and finish collecting samples for post-mortem analysis including histopathology and phosphoproteomics, RNA- and ChIP-seq analysis (Completion of Milestone #2, Major Task #3, and provide necessary information to add to our accomplished Milestone #3). We will also complete *in vitro* and *in vivo* drug combination experiments (Subtasks 1 and 2 in Major Task 6) with Dr. Drake's lab.

IMPACT

What was the impact on the development of the principal discipline(s) of the project?
Nothing to report.

What was the impact on other disciplines?
Nothing to report.

What was the impact on technology transfer?
Nothing to report.

What was the impact on society beyond science and technology?
Nothing to report.

CHANGES/PROBLEMS

Changes in approach and reasons for change

1. In **major task 1** we highlighted issues with overall survival of our GEMMs harboring the RET-GFP allele (most dying before 30 weeks of age).

2. In **major task 2** we have moved away from the LNCaP model grown in charcoal stripped serum as the results are too variable. We have since moved to use other prostate cancer cell line models that represent AVPC such as NCI-H660 and PC-3. We have now created shRNA RET knockdown lines from these cell lines and assessing functionally the role of RET and also creating RET overexpressed cell lines in 22Rv1 and LNCaP cells. This has delayed our progress a bit but we are catching up quickly.

Actual or anticipated problems or delays and actions or plans to resolve them

1. Overall, there was a significant delay in research productivity due to the coronavirus pandemic. University laboratories were shut down for 3 months and re-opened at minimal capacity for the next 3 months resulting in 6 months of significantly reduced research progress. Hence, we spent a big part of the first 3 months of the pandemic publishing our manuscript and the next 3 months ramping up our research program to get back to pre-pandemic levels as best as we can based on university policies. While we are not at pre-pandemic levels for productivity, we are getting up to speed and beginning to do research again.

2. We have generated a number of mice (Table 1) that we hope to age between 28-30 weeks to satisfy major task 1. As backup – we have generated 3D organoids from our GEMMs and in the process of making 2D cell lines. Further, we have used CRISPR-Cas9 to KO Ret from already established Pten:Rb1 double KO 2D cell lines. These models will guarantee us the ability to finish major task 1 if the GEMM models to not allow this.

Changes that had a significant impact on expenditures
None of the changes described above will result in >25% change in budget allocation, however, research spending is down due to the coronavirus pandemic as laboratories have been shut down.

Significant changes in use or care of human subjects, vertebrate animals, biohazards, and/or select agents
Nothing to report.

PRODUCTS
Publications, conference papers, and presentations

Journal publications
1. VanDeusen H, Ramroop JR, Morel KL, Bae S, Sheahan AV, Sychev Z, Lau NA, Cheng LC, Tan VM, Li Z, Petersen A, Lee JK, Park JW, Yang R, Hwang JH, Coleman I, Witte ON, Morrissey C, Corey E, Nelson PS, **Ellis L**, **Drake JM** (2020) Targeting RET Kinase in Neuroendocrine Prostate Cancer. *Mol Cancer Res*. 18(8):1176-1188.

Books or other non-periodical, one-time publications
Nothing to report.

Other publications, conference papers, and presentations
National Presentations:
Dr. Drake: Department of Microbiology, Immunology, and Cancer Biology Seminar, University of Virginia, Charlottesville, VA, "The RET kinase pathway as a target in neuroendocrine prostate cancer." – Canceled due to COVID-19

Dr. Drake: AACR Special Conference on Advances in Prostate Cancer Research, Denver, CO, "RET kinase as a driver of neuroendocrine prostate cancer." – Canceled due to COVID-19

Website(s) or other Internet site(s)
Nothing to report.

Technologies or techniques
Nothing to report.

Inventions, patent applications, and/or licenses
Nothing to report.

Other Products
Nothing to report.

PARTICIPANTS AND OTHER COLLABORATING ORGANIZATIONS

What individuals have worked on the project?

Name:	Dr. Leigh Ellis
Project Role:	Co-Principal Investigator
Researcher Identifier (e.g. ORCID ID):	0000-0003-4739-5049
Nearest person month worked:	
Contribution to Project:	Co-PI
Funding Support:	NCI, DOD

Name:	Dr. Yuzhen Zhou
Project Role:	Post-doc
Researcher Identifier (e.g. ORCID ID):	
Nearest person month worked:	3
Contribution to Project:	Post-doc researcher
Funding Support:	N/A

Name:	Dr. Justin M. Drake
Project Role:	Co-Principal Investigator
Researcher Identifier (e.g. ORCID ID):	
Nearest person month worked:	
Contribution to Project:	Co-PI
Funding Support:	DOD

Name:	Dr. Halena VanDeusen
Project Role:	Post-doc
Researcher Identifier (e.g. ORCID ID):	
Nearest person month worked:	12
Contribution to Project:	Post-doc researcher
Funding Support:	

Name:	Dr. Song Yi Bae
Project Role:	Post-doc
Researcher Identifier (e.g. ORCID ID):	
Nearest person month worked:	4
Contribution to Project:	Post-doc researcher
Funding Support:	

Has there been a change in the active other support of the PD/PI(s) or senior/key personnel since the last reporting period?
Nothing to report.

What other organizations were involved as partners?
Nothing to report.

SPECIAL REPORTING REQUIREMENTS
None

APPENDICES

- Figure 1-7
- Table 1
- References
- Manuscript (VanDeusen et al)

Figure 1: Observed Complication in Mice Expressing RET-GFP Alleles. Examples necropsy pictures Pten:Rb1:RET-GFP genetically engineered mice demonstrate long term survival complications including hypertrophied kidney (left: red arrow) and enlarged intestine indicating blockage (right: yellow arrow).

	Alive	Harvested	total
Ret(+/+)	11	3	14
Ret(+/lox)	11	7	18
Ret(lox/lox)	2	4 (1)	7

Table 1: Total number of mice with Pten:Rb1 double-out and differing RET zygosities for final analysis

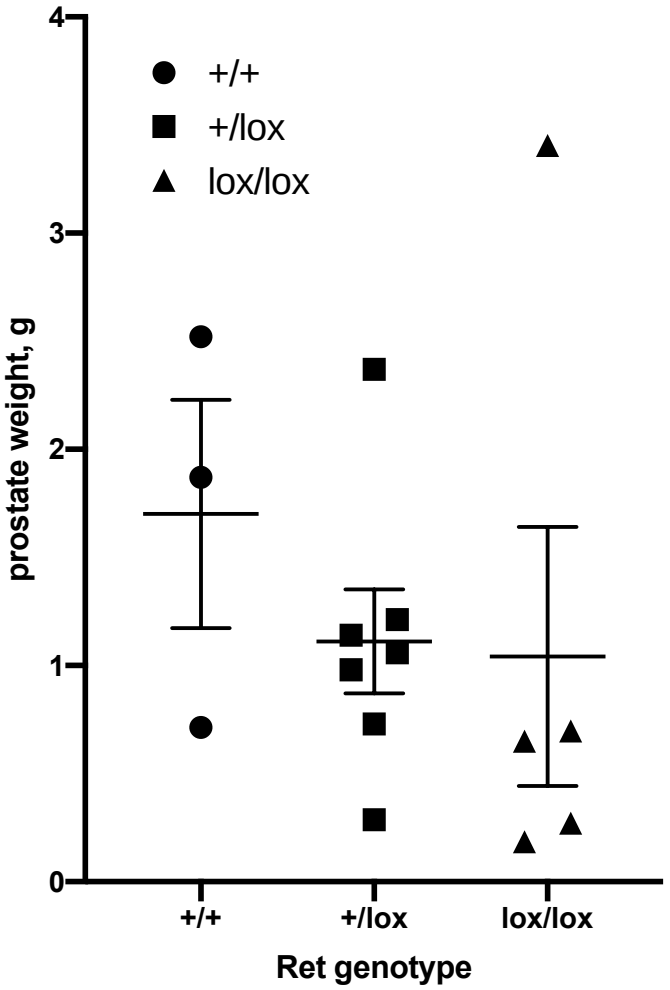

Figure 2: Assessing Affect of RET Function on Prostate Cancer Growth. Overall prostate gland weight from Pten:Rb1 double knockout GEMMs with indicated RET zygosity. Wild-type (+/+), Heterozygous (+/lox), Homozygous (lox/lox).

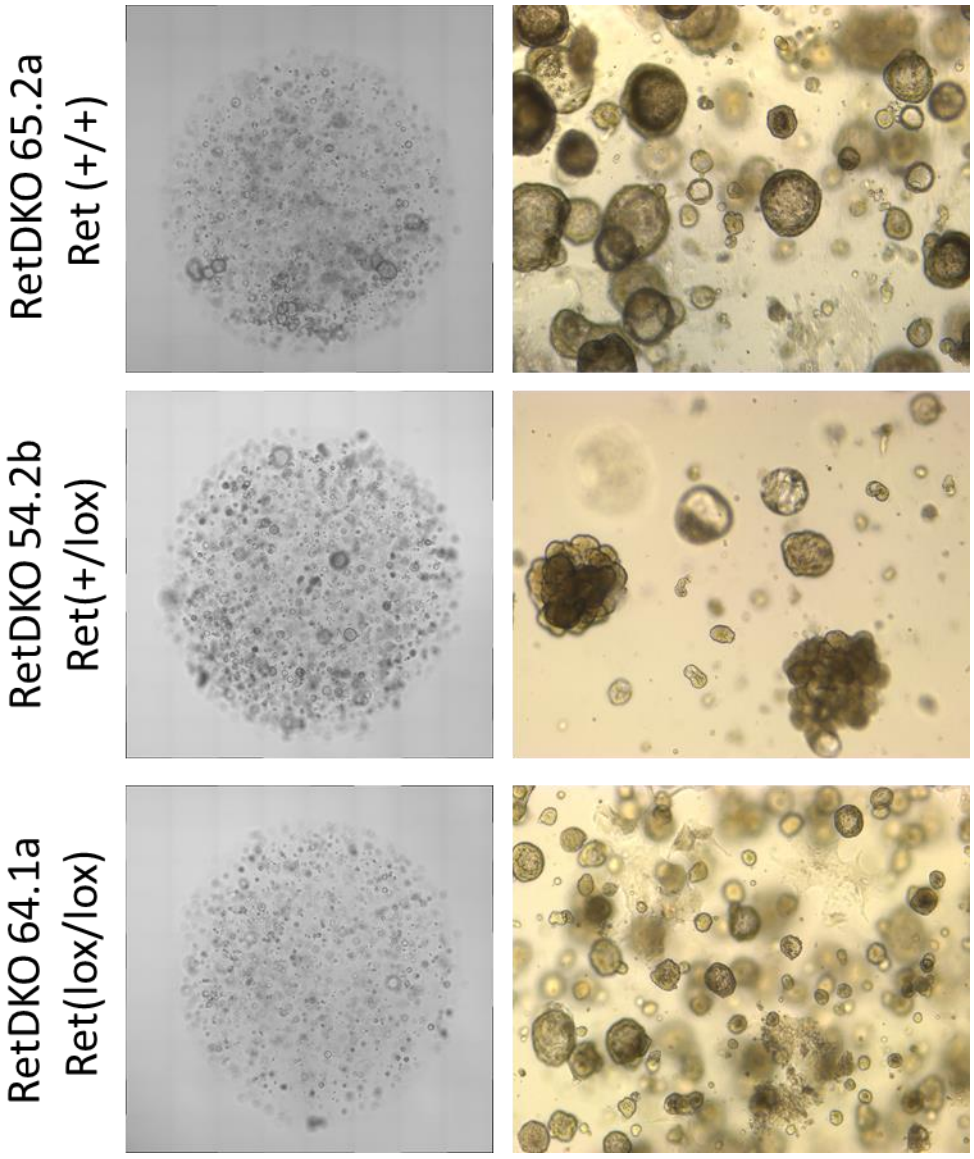

Figure 3: Assessing Affect of RET Function on Prostate Cancer Growth. Example pictures of organoid cultures from Pten:Rb1 double knockout (DKO) GEMMs with indicated RET zygosity. Wild-type (+/+), Heterozygous (+/lox), Homozygous (lox/lox).

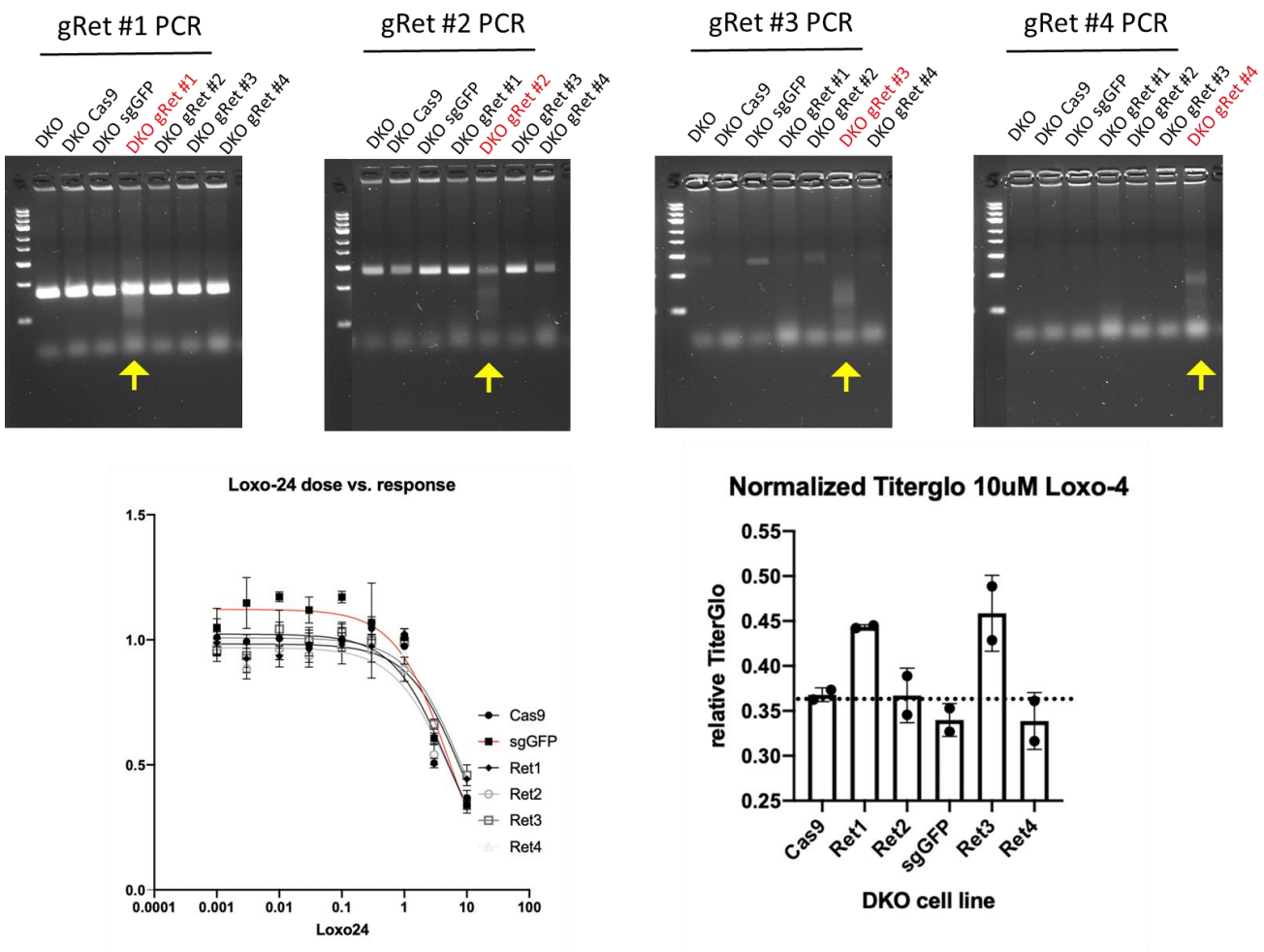

Figure 4: Assessing Affect of RET KO by CRISPR-Cas9 in Pten:Rb1 double-knockout (DKO) mouse 2-dimensional cell lines. Top Row – Genomic DNA was isolated from DKO-CRISPR-Cas9 cell lines post mock infection or infection with control guide (sgGFP) or four independent specific targeted Ret guides (gRet). Following PCR amplification, it is observed that each Ret targeted guide is specific and all generate indels (yellow arrows) indicating specific activity. Bottom Row (left) – All indicated cell lines we treated with increasing concentrations with a specific RET inhibitor – Loxo292. Analysis of response was determined by use of Cell Titerglo assay. (Right) Demonstration of differing response of indicated cell lines demonstrating that targeting Ret expression with guide 1 (Ret1) and guide 3 (Ret 3) may provide adequate loss of Ret expression/function for cells to aquire resistance to chemical inhibitors of Ret kinase.

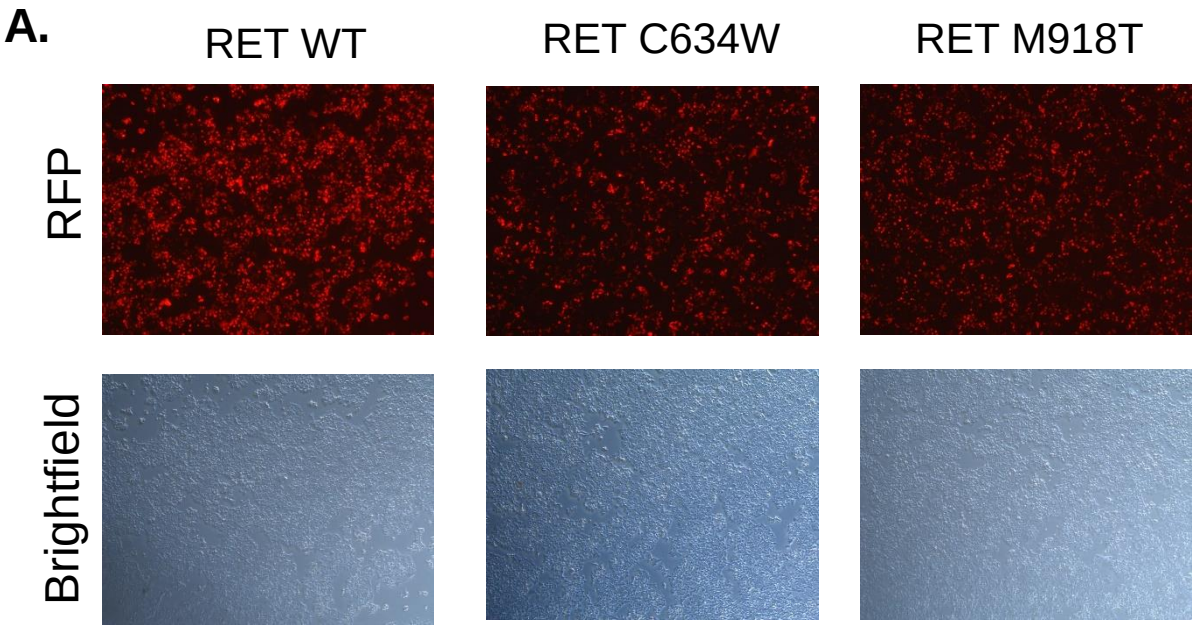

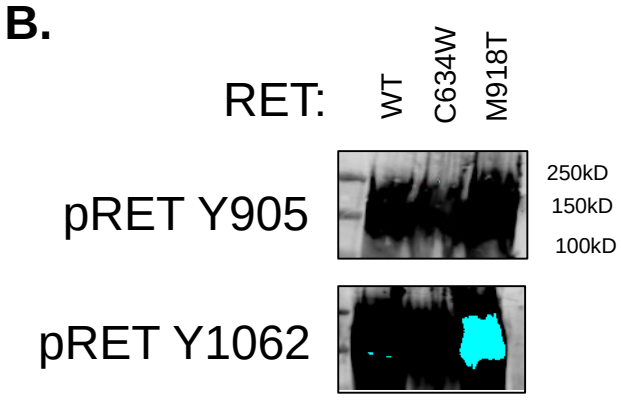

Figure 5. A. 10ug of RET overexpression constructs (WT: wild type RET, C634W and M918T: constitutively active mutants) were transfected into HEK-293T cells and images were taken 24 hours post transfection. Red Fluorescent Protein (RFP) is co-expressed with the RET protein and serves as a positive control for transfection. B. Lysates from cells imaged in A. were collected analyzed by western blot. The blots show robust expression and phospho-specific antibodies show phosphorylation indicative of of RET kinase activity at residues Y905 and Y1062. Validation of the constructs in 293T cells allows us to move forward with overexpression in LNCaP cells as part of the experiments for Major Task 2.

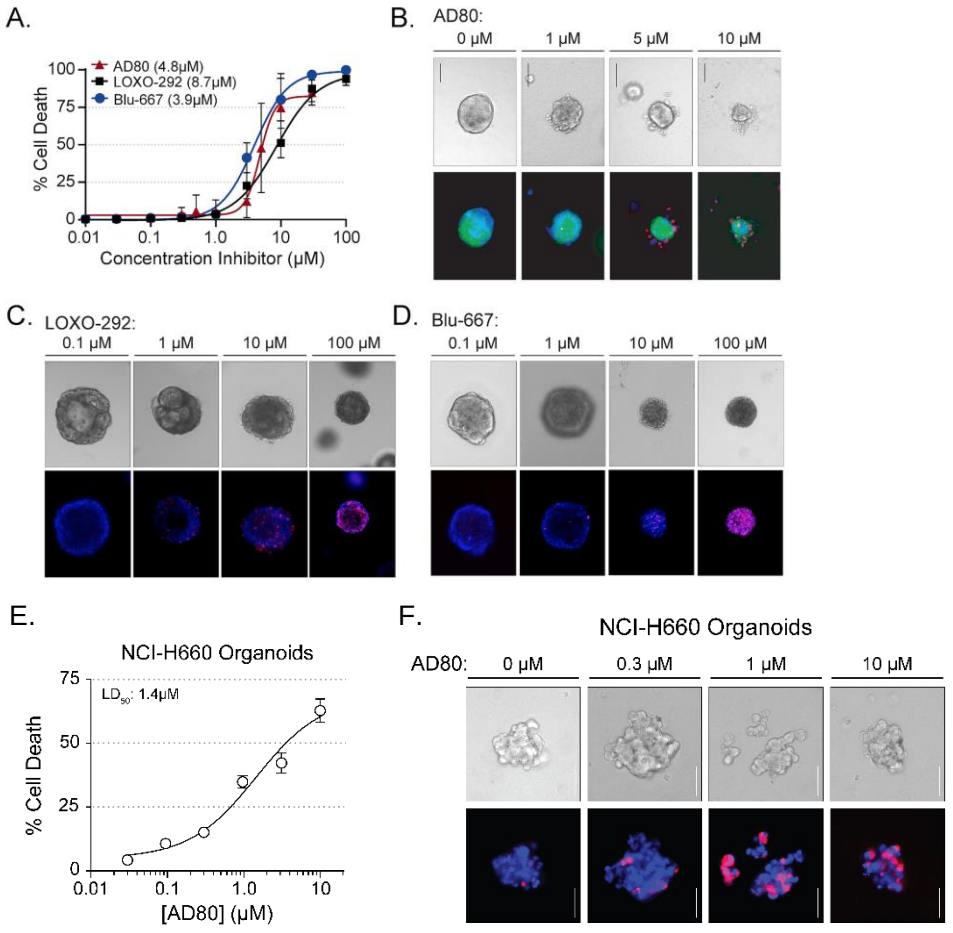

Figure 6. A. AVPC tumors modeled by Pten/ and Rb/ prostate specific double knockout (DKO) and grown as organoids were treated with RET inhibitors: AD80, LOXO-292, and BLU-667. Effect of the drug was measured by cell viability. Viability was measured by PI staining for dead cells. Circles represent mean and error bars with SD. B. Bright field images and corresponding fluorescence images of GFP-labeled DKO organoids treated with the indicated concentrations of AD80. Blue, DAPI staining of nuclei; red, propidium iodide staining of dead cells. Scale bar, 100 mm. Representative brightfield and fluorescent images of LOXO-292 (C) and BLU-667 (D) DKO organoids treated with the indicated concentrations of drugs stained as described with the GFP channel omitted. E. NCI-H660 cells were grown as organoids and treated with increasing concentrations of AD80, which increases the percentage of cell death. F. Images of NCI-H660 organoids treated with AD80 as in B.

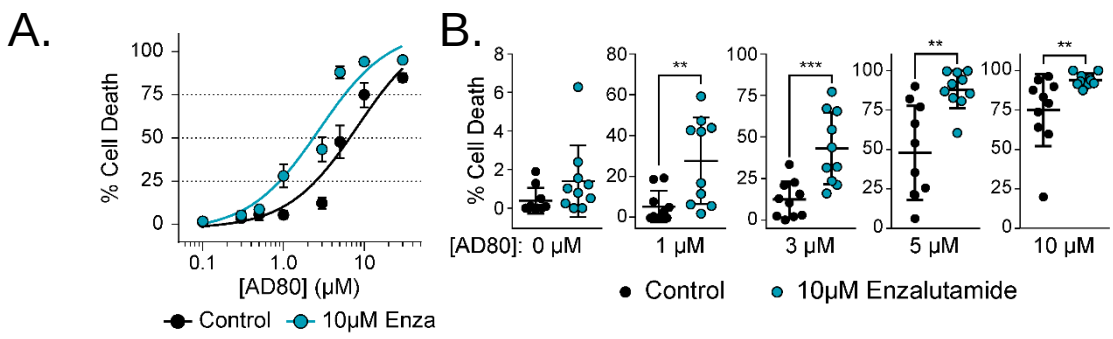

Figure 7. A. Pten-/- and Rb-/- prostate specific double knockout (DKO) and grown as organoids were treated with 10uM enzalutamide and RET inhibitor AD80. Effect of the drug was measured by cell viability. Viability was measured by PI staining for dead cells. Circles represent mean and error bars with SD. B. Individual drug treatment doses and percent viability for each organoid measured are shown in individual graphs. The 0uM AD80 treatment group shows enzalutamide alone has no effect on viability of DKO organoids. However, with increasing concentration of the RET inhibitor, enzalutamide treatment further increases the percentage of cell death.

REFERENCES

1. VanDeusen, H.R., *et al.* Targeting RET Kinase in Neuroendocrine Prostate Cancer. *Mol Cancer Res* (2020).
2. Ku, S.Y., *et al.* Rb1 and Trp53 cooperate to suppress prostate cancer lineage plasticity, metastasis, and antiandrogen resistance. *Science* **355**, 78-83 (2017).

Targeting RET Kinase in Neuroendocrine Prostate Cancer

Halena R. VanDeusen[1], Johnny R. Ramroop[2], Katherine L. Morel[3], Song Yi Bae[1], Anjali V. Sheahan[3], Zoi Sychev[1], Nathan A. Lau[4], Larry C. Cheng[5], Victor M. Tan[5], Zhen Li[6], Ashley Petersen[7], John K. Lee[4,8], Jung Wook Park[9,10], Rendong Yang[11], Justin H. Hwang[12,13], Ilsa Coleman[4], Owen N. Witte[10], Colm Morrissey[14], Eva Corey[14], Peter S. Nelson[4,8], Leigh Ellis[3,13], and Justin M. Drake[1,15,16]

ABSTRACT

The increased treatment of metastatic castration-resistant prostate cancer (mCRPC) with second-generation antiandrogen therapies (ADT) has coincided with a greater incidence of lethal, aggressive variant prostate cancer (AVPC) tumors that have lost dependence on androgen receptor (AR) signaling. These AR-independent tumors may also transdifferentiate to express neuroendocrine lineage markers and are termed neuroendocrine prostate cancer (NEPC). Recent evidence suggests kinase signaling may be an important driver of NEPC. To identify targetable kinases in NEPC, we performed global phosphoproteomics comparing several AR-independent to AR-dependent prostate cancer cell lines and identified multiple altered signaling pathways, including enrichment of RET kinase activity in the AR-independent cell lines. Clinical NEPC patient samples and NEPC patient-derived xenografts displayed upregulated RET transcript and RET pathway activity. Genetic knockdown or pharmacologic inhibition of RET kinase in multiple mouse and human models of NEPC dramatically reduced tumor growth and decreased cell viability. Our results suggest that targeting RET in NEPC tumors with high RET expression could be an effective treatment option. Currently, there are limited treatment options for patients with aggressive neuroendocrine prostate cancer and none are curative.

Implications: Identification of aberrantly expressed RET kinase as a driver of tumor growth in multiple models of NEPC provides a significant rationale for testing the clinical application of RET inhibitors in patients with AVPC.

Introduction

Second-generation ADT, such as abiraterone acetate and enzalutamide, have provided life-extending therapies for patients with recurrent or mCRPC. However, the utilization of more effective ADT has coincided with an increase in the development of AVPC (1). This subset of mCRPC is characterized by poor prognosis and loss of AR signaling (2). The absence of AR signaling in AVPC renders the existing hormone targeting treatments ineffective and remaining approved therapies, including platinum-based chemotherapy, offer only limited therapeutic benefits (3). A subset of AVPC tumors are classified as NEPC because they express neuroendocrine genes, which are not typically expressed in prostate adenocarcinoma. Recent work has implicated the loss of *RB1* and *TP53* mutations as key alterations in the development of NEPC, and inhibition of kinases such as Aurora A kinase (AURKA), MAPK, or FGFR could provide therapeutic opportunities if selected in the right patient subsets (1, 4–6). Even with these new developments, there still remains a critical need to understand the molecular characteristics and kinase signaling pathways of NEPC tumors to identify and validate effective treatment options.

Receptor tyrosine kinases link the extracellular environment to intracellular responses through multiple signaling cascades. These signaling cascades regulate numerous pathways that are frequently altered in transformed cells, including cell growth, metabolism, proliferation, differentiation, invasion, motility, and cell death (7). RET is a receptor tyrosine kinase that is essential for neural crest development and is frequently mutated or translocated in subsets of endocrine tumors such as multiple endocrine neoplasia 2 (MEN2) and papillary thyroid carcinomas, respectively (8). RET can be therapeutically targeted with some success in these tumor types. Recently, RET kinase was identified to be tyrosine phosphorylated in a CRPC patient with small-cell neuroendocrine pathology (9) and as an enriched cell surface marker in NEPC (10). Furthermore, RET knockdown reduced tumor growth of an AR-dependent cell line xenograft, LNCaP, *in vivo* (11). However, whether RET inhibition could be exploited

[1]Department of Pharmacology, University of Minnesota-Twin Cities, Minneapolis, Minnesota. [2]Departments of Cancer Biology and Genetics, Comprehensive Cancer Center, The Ohio State University, Columbus, Ohio. [3]Department of Oncologic Pathology, Dana-Farber Cancer Institute, Boston, Massachusetts. [4]Division of Human Biology, Fred Hutchinson Cancer Research Center, Seattle, Washington. [5]Graduate Program in Quantitative Biomedicine, School of Graduate Studies, Rutgers University, New Brunswick, New Jersey. [6]Cancer Metabolism and Growth Program, Rutgers Cancer Institute of New Jersey, New Brunswick, New Jersey. [7]Division of Biostatistics, School of Public Health, University of Minnesota-Twin Cities, Minneapolis, Minnesota. [8]Department of Medicine, University of Washington, Seattle, Washington. [9]Department of Pathology, Duke School of Medicine, Duke University, Durham, North Carolina. [10]Department of Microbiology, Immunology, and Molecular Genetics, University of California–Los Angeles, Los Angeles, California. [11]The Hormel Institute, University of Minnesota, Austin, Minnesota. [12]Department of Medical Oncology, Dana-Farber Cancer Institute, Boston, Massachusetts. [13]Broad Institute of Harvard and MIT, Cambridge, Massachusetts. [14]Department of Urology, University of Washington, Seattle, Washington. [15]Department of Urology, University of Minnesota-Twin Cities, Minneapolis, Minnesota. [16]Masonic Cancer Center, University of Minnesota-Twin Cities, Minneapolis, Minnesota.

Note: Supplementary data for this article are available at Molecular Cancer Research Online (http://mcr.aacrjournals.org/).

H.R. VanDeusen and J.R. Ramroop contributed equally to this article.

Corresponding Author: Justin M. Drake, University of Minnesota Medical School, 6-120 Jackson Hall, 321 Church St SE, Minneapolis, MN 55455. Phone: 612-624-7151; E-mail: jdrake@umn.edu

Mol Cancer Res 2020;XX:XX–XX

doi: 10.1158/1541-7786.MCR-19-1245

as a therapeutic target in the treatment of neuroendocrine prostate cancer is unknown.

Here, we evaluated the phosphoproteome of multiple AR-independent and AR-dependent prostate cancer cell lines to identify altered kinase signaling pathways that are unique to AR-independent prostate cancers. Several downstream signaling networks of RET kinase, and RET kinase itself, were enriched and activated in the AR-independent cell lines when compared with AR-dependent cell lines. In addition, RET kinase was overexpressed in NEPC tumors in multiple clinical datasets. We found that the NEPC cell line, NCI-H660, was dependent on RET expression for proliferation and that targeted RET pathway inhibitors, AD80, and two other inhibitors currently being evaluated in the clinic, LOXO-292 and BLU-667 (12, 13), potently induced cell death more effectively than currently approved RET inhibitor therapies, cabozantinib and vandetanib (14, 15). Finally, we found that AD80, LOXO-292, and BLU-667, were effective in inducing cell death in NEPC organoid models and AD80 was able to reduce tumor growth of NEPC xenograft tumor models. These results indicate that RET kinase is required for tumor growth of several models of NEPC, and that inhibiting RET induces cell death in neuroendocrine prostate cancer cells that are resistant to current ADT therapies. These results ultimately nominate RET as a key candidate to test further in the development and effective treatment of NEPC.

Materials and Methods

Phosphoproteomics of prostate cancer cell lines

Cultured prostate cancer cells were scraped, pelleted, and snap frozen. Phosphopeptide enrichment and trypsin digestion were performed as described previously (16). Briefly, cells were lysed in 6 mol/L guanidium hydrochloride buffer (6 mol/L guanidinium chloride, 100 mmol/L Tris pH 8.5, 10 mmol/L Tris (2-carboxyethyl) phosphine, 40 mmol/L 2-chloroacetamide, 2 mmol/L Vanadate, 2.5 mmol/L sodium pyrophosphate, 1 mmol/L Beta-glycerophosphate, 10 mg/mL N-octyl-glycoside), sonicated, and cleared. Five milligrams of total protein was digested with trypsin and a 4G10 antibody–based immunoprecipitation (IP) was used to enrich phosphotyrosine peptides. The IP supernatant containing the phosphoserine/threonine (pS/T) peptides (2.5 mg) were desalted on C18 columns and separated via strong cation exchange chromatography. In separate, parallel reactions the pY and pS/T peptides were enriched from nonphosphorylated peptides using titanium dioxide columns. Finally, the pY and pS/T peptides were each desalted with C18 tips prior to mass spectrometer analysis (LC/MS-MS with a dual pump nanoRSLC system (Dionex) interfaced with a Q Exactive HF (Thermo Fisher Scientific; ref. 17). Technical duplicates were run for all samples and data were analyzed using MaxQuant Andromeda version 1.5.3.30 (parameter settings in ref. 18) against the Uniprot human reference proteome database with canonical and isoform sequences (downloaded September 2016 from http://uniprot.org). Datasets are accessible through dataset identifiers PXD012970 and PXD012971 (19) through the ProteomeXchange Consortium via the PRIDE partner repository.

Phosphoproteome MS data analysis was performed as described previously (20). For supervised clustering, pY and pS/T data were filtered using a 4-fold change cutoff comparing NEPC versus adenocarcinoma from the original excel tables (See Supplementary Tables S2 and S3). We expanded upon our previously published mCRPC dataset (PXD002286) by decreasing the phosphosite localization probability cutoff from 0.99 to 0.75 (16). This increased our identifications nearly 50% and have now reported those extra identifications in this manuscript as Supplementary Table S6. Hierarchical clustering was performed on mass spectrometry and gene expression data using Cluster (Version 3.0) with the Pearson correlation and pairwise complete linkage analysis (21). Java TreeView version 1.1.6r4 was used to visualize clustering results (22).

Kinase substrate enrichment analysis

KSEA was performed as described previously (23). Briefly, phosphopeptides were rank-ordered by average fold change between AR-independent (AVPC) versus AR-dependent (adenocarcinoma) prostate cancer cell lines. An enrichment score was calculated using the Kolmogorov–Smirnov statistic and statistical significance was calculated via permutation analysis. The normalized enrichment score (NES) was calculated by taking the enrichment score and dividing by the mean of the absolute values of all enrichment scores from the permutation analysis. The Benjamini–Hochberg procedure was utilized to calculate false discovery rate for each kinase. For pY analyses, cutoffs of FDR<0.05, hits>4, and NES>1.3 were used. For pS/T analyses, cutoffs of FDR<0.02, hits>5, and NES>2 were used.

Tissue culture

Human prostate cancer cell lines LNCaP, VCaP, C4-2, 22Rv1, DU-145, PC3, and NCI-H660 cells were obtained from the ATCC. Cell lines were validated annually by Promega PowerPlex16HS Assay at the University of Arizona Genetics core and cells were tested for Mycoplasma contamination by PCR amplification every three months (24). Cells were not used beyond fifteen passages without reauthentication. LNCaP, VCaP, C4-2, 22Rv1, DU145, and PC3 cells were grown in appropriate media as recommended by ATCC (Life Technologies) supplemented with 10% FBS (Sigma-Aldrich) and 1% penicillin–streptomycin (Life Technologies). NCI-H660 cells were grown in Advanced DMEM/F12 (Gibco), with 1× B27 Supplement (Gibco), 10 ng/mL EGF (PeproTech), 10 ng/mL bFGF (PeproTech), and 1% penicillin–streptomycin 1× Glutamax (Life Technologies). LASCPC-01, cMyc/myrAKT, PARCB-1-3, and -5, and EF1 cell lines were obtained from Dr. Owen Witte at UCLA and cultured as described previously (10, 25–27). H660 organoids were cultured as described in ref. 28. Mouse organoids were established by enzymatic digestion of GEMM primary prostate tumor tissue in 5 mg/mL Collagenase type II (Gibco) in DMEM/F12 (Gibco) media with 10 μmol/L Y-27632 dihydrochloride (Tocris Bioscience). Digested cells were seeded into 100% Matrigel and cultured as described by Drost and colleagues 2016 (ref. 28). NCI-H660 organoids were seeded into Prostate 18 QGel 3D Matrix (QGel) according to manufacturer's instructions and cultured in RPMI-HITES media with B27 supplement (Gibco), 1.25 mmol/L N-acetylcysteine (Sigma), 5 ng/mL EGF (PeproTech), 500 nmol/L A83-01 (Tocris Bioscience), 5 ng/mL FGF2 (PeproTech), 10 ng/mL FGF10 (PeproTech), 10 mmol/L Nicotinamide (Sigma), and 1 μmol/L Prostaglandin E2 (Tocris Bioscience). Culture media was replenished every 4 days and organoids were passaged by sequential digestion in 1 mg/mL Dispase II (Gibco) followed by TrypLE Express (Gibco) and mechanical disruption through a needle to dissociate to single cells before resuspension as a 3D culture. RET immunofluorescence in SKO and DKO organoids was followed standard staining procedures using the RET antibody (Cell Signaling Technology E1N8X, 1:100). All cells were grown and maintained in a humidified incubator at 37°C and 5% CO_2.

Dependency analysis

Gene dependency data is based on pooled genome-scale shRNA screens from DEMETER-adjusted (29) Project Achilles 2.201 data (30). DEMETER scores for RET was ranked for all cell lines was ranked and

plotted across 503 cell lines. Of the same data, to statistically compare the patterns of RET dependency in 8 prostate cancer cell lines to other genes, we ranked the DEMETER score of 11,280 genes in eight prostate cell lines and computed the spearman correlation coefficient for each gene dependency relative to RET dependency.

Generating stable RET knockdown cell lines and cell growth assay

pLKO.1 scramble shRNA and shGFP plasmids were a gift from David Sabatini (Addgene plasmid #1864 and #30323) and two pLKO.1 –shRET plasmids (RET1: CCACCCACATGTCATCAAATT, RET2: GGGCGACCGTACATGACTATA) used to generate the Project Achilles dataset were kindly provided by laboratory of Dr. William C. Hahn (Dana-Farber Cancer Institute, Boston, MA) from the RNAi Consortium at the Broad Institute. Lentiviral particles were generated by transfecting 293T cells with 13 μg pMDL, 5 μg pRev, 7 μg pVSVg, and 20 μg pLKO.1 shRNA plasmid using calcium phosphate. NCI-H660 or PC3 cells were transduced with lentivirus in the presence of polybrene (10 μg/mL). After 72 hours of infection, stable cells were selected by puromycin (0.5 μg/mL for NCI-H660 cells; 1 μg/mL for PC3 cells).

Stable cells were seeded into 96-well plates at cell density of 1,000 cells/well ($n = 5$) for NCI-H660–derived cell lines and 200 cells/well ($n = 3$) for PC3-derived cell lines. Then, cells were cultured for indicated length of days. Cell culture media of NCI-H660 and PC3-derived stable cell lines was replenished every 5 days or 3 days, respectively. Cell proliferation was measured every 5 days for NCI-H660–derived stable cell lines and every 2 to 3 days for PC3-derived stable cell lines using WST reagent (Takara).

Immunoprecipitation and Western blots

Cells for Western blot analysis were lysed with 1% SDS/2% β-mercaptoethanol (β-ME) and boiled for 10 minutes following a freeze thaw after lysis. The protein concentration was determined using Bio-Rad Quick Start Bradford Protein Assay Kit following manufacturer's protocol. Twenty micrograms of protein per lane was loaded into GenScript SurePage 4% to 12% gel, transferred to a nitrocellulose membrane, blocked in 5% BSA in 1xTBST for one hour at room temperature before incubating in primary antibodies (diluted in 1% BSA in TBST) overnight at 4°C. Membranes were washed with 1× TBST before incubating in LI-COR IR-conjugated secondary antibodies (diluted 1:5,000) for 1 hour at room temperature, washed again and imaged using the LI-COR Odyssey System and adjusted with the LI-COR Image Studio Lite software (v5.2). The following antibodies were used for Western blot analysis at 1:1,000 fold dilutions unless otherwise indicated: Total RET (Cell Signaling Technology E1N8X), phospho-ERK1/2 T202/Y204 (Cell Signaling Technology D13.14.4E), total ERK1/2 (Cell Signaling Technology 137F5), pAKT1/2 S473 (Cell Signaling Technology D9E), AKT (Cell Signaling Technology, C67E7), phospho-tyrosine (Millipore Sigma 4G10, 1:500), AR (Santa Cruz Biotechnology, sc-7305, 1:500), α-Tubulin (Santa Cruz Biotechnology, sc32233), and β-actin (Cell Signaling Technology 13E5, 1:5,000).

For immunoprecipitation analysis, cells were lysed with cell lysis buffer containing 20 mmol/L Tris-HCl (pH 7.5), 150 mmol/L NaCl, 1 mmol/L Na_2EDTA, 1 mmol/L EGTA, 1% Triton, 2.5 mmol/L sodium pyrophosphate, 1 mmol/L beta-glycerophosphate, 1 mmol/L Na_3VO_4, 1 μg/mL leupeptin, and 1 mmol/L phenylmethylsulfonylfluoride. The protein concentration was determined by bicinchoninic acid protein assay (Pierce) according to the manufacturer's instructions. The immunoprecipitation was performed using Dynabeads Protein A (Life Technologies) following the manufacturer's protocol with modification. Briefly, total RET (Cell Signaling Technology C31B4, 1:50) antibody was preincubated with the beads overnight at 4°C. Then, equal amount of each cell lysate was incubated with the RET antibody–conjugated beads overnight at 4°C. After washing the bead–RET antibody–antigen complex four times with cell lysis buffer, the antigen was eluted with 2× Laemmli Sample Buffer (Bio-Rad)/5% β-ME by heating at 95°C for 5 minutes before analysis by Western blot analysis.

LD_{50} value measurement

AD80, BLU-667, cabozantinib, and vandetanib were all obtained from Selleckchem and LOXO-292 was obtained from MedChemExpres. All drugs were resuspended in DMSO. Cells were treated with drug for 72 hours prior to the WST assay and viability was measured using the WST reagent (Takara) following manufacturer's protocol. Each concentration data point was conducted in triplicate. Each compound was tested at a minimum of ten dose levels, separated by 4-fold dilution concentration intervals, LD_{50} values were calculated using GraphPad Prism 7. Reported values were calculated from a single WST assay, but were confirmed by repeating the entire assay in duplicate.

Organoid dose response

For assays, organoids were seeded as single cells in 40 μL of 33% Matrigel (mouse organoids) or Prostate 18 QGel 3D Matrix (NCI-H660 organoids) in 96-well tissue culture plates and cultured for 2 days at 37°C to allow organoid formation. Once formed, organoids were treated with AD80 (at concentrations of ranging from 0.1 μmol/L to 30 μmol/L), LOXO-292 or BLU-667 (at concentrations ranging from 0.01 μmol/L to 100 μmol/L), or 10 μmol/L enzalutamide (MedchemExpress) for 72 hours. After treatment, cells were stained with 10 μL ReadyProbes Cell Viability Imaging Kit Blue/Red (Invitrogen) per well for 30 minutes at room temperature and z-stack images of stained cells were taken using an EVOS FL Auto 2 Cell Imaging System (Invitrogen). The percentage of cell death was calculated by identifying the percentage of PI-positive cells per organoid in at least 10 organoids for each treatment condition and the LD_{50} was calculated in GraphPad Prism 7.

In vivo studies

Experiments were carried out on 8-week-old male NOD-SCID mice in accordance with Institutional Animal Care and Use Committee (IACUC)-approved protocols at Rutgers University (New Brunswick, NJ). Xenografts were generated via subcutaneous injection of 1×10^6 NCI-H660 cells per animal mixed at a 1:1 ratio with Corning Matrigel Matrix into the right flank. Tumors were allowed to grow to approximately 100–200 mm^3 before mice were randomly allocated into vehicle (5% DMSO) or AD80 (10 mg/kg/day in the first experiment or 20 mg/kg/day in the second experiment) treatment groups. Dosing proceeded once daily, 5 days a week for 22 days by oral gavage. Tumor volume and animal weight were measured every two days. Tumors volume was measured by caliper and expressed in mm^3 (tumor volume $= 0.5\ a \times b^2$, where a and b represents long and short diameter, respectively) and maximal tumor volume permitted by Rutgers University IACUC was never exceeded.

IHC

Xenograft tumors were formalin-fixed paraffin-embedded and sectioned following standard procedure. To stain, sections were deparaffinized by baking at 65°C for 1 hour and hydrated with sequential washes in xylenes, 100% ethanol, 95% ethanol, 70% ethanol, and 1× PBS, prior to citrate buffer pH 6.0 antigen retrieval. To stain,

tissues were washed with 0.1% TBST, blocked with 2.5% normal horse serum for 1 hour at room temperature before incubating in primary antibody (RET: Cell Signaling Technology E1N8X, 1:500 and Ki67: Cell Signaling Technology 8D5, 1:400) overnight at 4°C in a humidified slide box. Slides were washed with 0.1% TBST and incubated in HRP-conjugated secondary antibody (Vector Laboratories, MP-7500-15) for 1 hour at room temperature and developed using a DAB peroxidase substrate kit (Vector Laboratories, NC9567138). Reaction was stopped with water before proceeding to counterstaining with hematoxylin for 1 minute. Slides were destained in tap water, dehydrated with ethanol and xylenes, and mounted. Tumor sections were imaged on a Zeiss Axiovert A2. Average RET or KI67 staining was determined by color deconvolution followed by measurement of the mean gray value in the DAB channel in Fiji (31). Mean gray value was converted to optical density with the following equation: OD = Log (Max gray value/Mean gray value). Values for images from five distinct fields of view were averaged to create a single data point for each tumor in each treatment group.

Terminal deoxynucleotidyl transferase dUTP nick end labeling assay

The Click-iT Plus TUNEL Assay for In Situ Apoptosis Detection, Alexa Fluor 488 Kit was used according to the manufacturer's protocol (Invitrogen). Nuclei were counterstained with Hoechst 33342 (Thermo Fisher Scientific). A DNase-treated positive control section was incubated in 1 U of DNase I diluted into 1× DNase I Reaction Buffer (20 mmol/L Tris-HCl, pH 8.4, 2 mmol/L $MgCl_2$, 50 mmol/L KCl) for 30 minutes at room temperature (Invitrogen). The Terminal deoxynucleotidyl transferase dUTP nick end labeling (TUNEL)-positive cells in tissue sample slides were identified by comparing with the DNase-treated positive control and the no-TdT enzyme negative control. Percent TUNEL-positive area was determined by using Fiji to measure the TUNEL-positive area divided by total tumor area × 100 for each tumor. Adjacent tissue sections were stained with hematoxylin and eosin by the University of Minnesota Clinical and Translational Science Institute Histology & Research Laboratory.

Statistical analysis

For xenograft tumor volume experiments, means and confidence intervals (CI) were calculated on the log scale due to skew and reported in terms of geometric means after exponentiation. Tumor growth rates were fit with a linear mixed effect model in R. All other statistical analyses and Pearson correlations were performed using GraphPad Prism 7 with the tests indicated in the figure legends. $P < 0.05$ was considered to indicate a statistically significant difference. P values were determined with significance indicated as follows: *, $P < 0.05$; **, $P < 0.01$; ***, $P < 0.001$; and ****, $P < 0.0001$.

Results

AR-independent cell lines have altered phospho-tyrosine and phospho-serine/threonine kinase signaling pathways

To identify the unique kinase signaling pathways required for growth and proliferation of AR-independent prostate cancer, we performed phospho-proteomic profiling. We compared AR-dependent cell lines (LNCaP, VCaP, C4-2, and 22Rv1), to AR-independent cell lines that are resistant to ADT and harbor mutations commonly found in NEPC tumor samples [DU145, PC3, NCI-H660, cMyc/myrAKT, LASCPC-01 (26), EF-1 (10), and PARCB-1,-2,-3, and -5 (27); Supplemental Fig. 1 and Supplementary Table S1]. Supervised hierarchical clustering between the AR-dependent and AR-independent groups revealed distinct patterns in phospho-serine/threonine (pS/T) and phospho-tyrosine (pY) peptides (**Fig. 1A** and **B**, respectively; Supplementary Tables S2 and S3). Kinase substrate enrichment analysis (KSEA) identified AURKA as the most highly enriched pS/T kinase (**Fig. 1C**) and this kinase has been previously reported to be significantly upregulated in NEPC (4). Interestingly, among the tyrosine kinases, RET kinase was also significantly enriched (**Fig. 1D**), suggesting that RET kinase is activated in AR-independent cell lines (full pS/T and pY KSEA results are in Supplementary Tables S4 and S5, respectively). We confirmed that the RET protein is highly upregulated in the NEPC subset of AR-independent cell lines (Supplementary Fig. S1). Further investigation into the RET pathway via our cell line–derived and previously published mCRPC rapid autopsy phosphoproteomic datasets (9) (expanded phosphoproteome dataset in Supplementary Table S6, see Materials and Methods) identified hyperphosphorylation and, in some cases, activation, of several RET pathway targets including MAPK, AKT, and STAT3 (**Fig. 1E** and **F**), further confirming RET pathway activity in AVPC cell lines and tumors.

RET kinase gene expression is upregulated in patients with neuroendocrine prostate cancer

We took advantage of several clinical prostate cancer gene expression datasets to determine whether RET kinase was overexpressed along with known markers of NEPC. Analysis of the University of Washington rapid autopsy dataset (32) which contains multiple metastatic tumors from patients with CRPC revealed that the NEPC (AR-negative, NE-positive) subset had enrichment of RET kinase expression concomitant with increased neuronal lineage genes ASCL1 and chromogranin A (CHGA) and decreased luminal epithelial lineage genes *AR, NKX3-1*, and *KLK3* expression (**Fig. 2A**). Among all patient samples included in the dataset, there was a strong correlation between levels of RET and neuronal lineage markers, while there was a negative correlation with RET expression and the AR-responsive genes (**Fig. 2B**). Overall, the NE-positive patient population had increased RET expression compared with the AR-positive population (**Fig. 2C**). An additional patient-derived xenograft (PDX) transcript dataset comparing metastatic NEPC to metastatic adenocarcinoma showed a similar correlation and upregulation of expression of RET and neuronal lineage markers in the NEPC population (**Fig. 2D–F**; ref. 33). This trend was also observed in additional prostate cancer datasets (Supplemental Fig. 2; refs. 6, 34–36). Overall, these independent datasets demonstrate that RET kinase is frequently overexpressed in clinical NEPC tumors and supports our cell line phosphoproteomic and KSEA analyses, suggesting enhanced RET activity drives NEPC proliferation and survival and therefore nominates RET as a candidate therapeutic target for NEPC tumors.

RET expression correlates with neuroendocrine transcription factors in prostate cancer cell lines and is necessary for NEPC proliferation

The robust levels of RET gene expression in NEPC patient samples suggests it is a potential target in NEPC. To validate the correlation of RET gene expression in prostate cancer cell lines, we examined relative RET dependency in the publicly available pooled genome-scale RNAi screen of 503 cancer cell lines, which includes seven prostate cancer cell lines and one basal prostate cell line (30). We compared the patterns of RET dependency relative to 11,280 genes in the eight prostate cell lines (Supplementary Table S7). As shown in **Fig. 3A**, strong correlations were observed between the dependencies of RET and NEPC driver genes (*POU3F2, SOX2, ONECUT2*, and *ASCL1*). In contrast, a negative correlation was seen between the dependencies of RET and

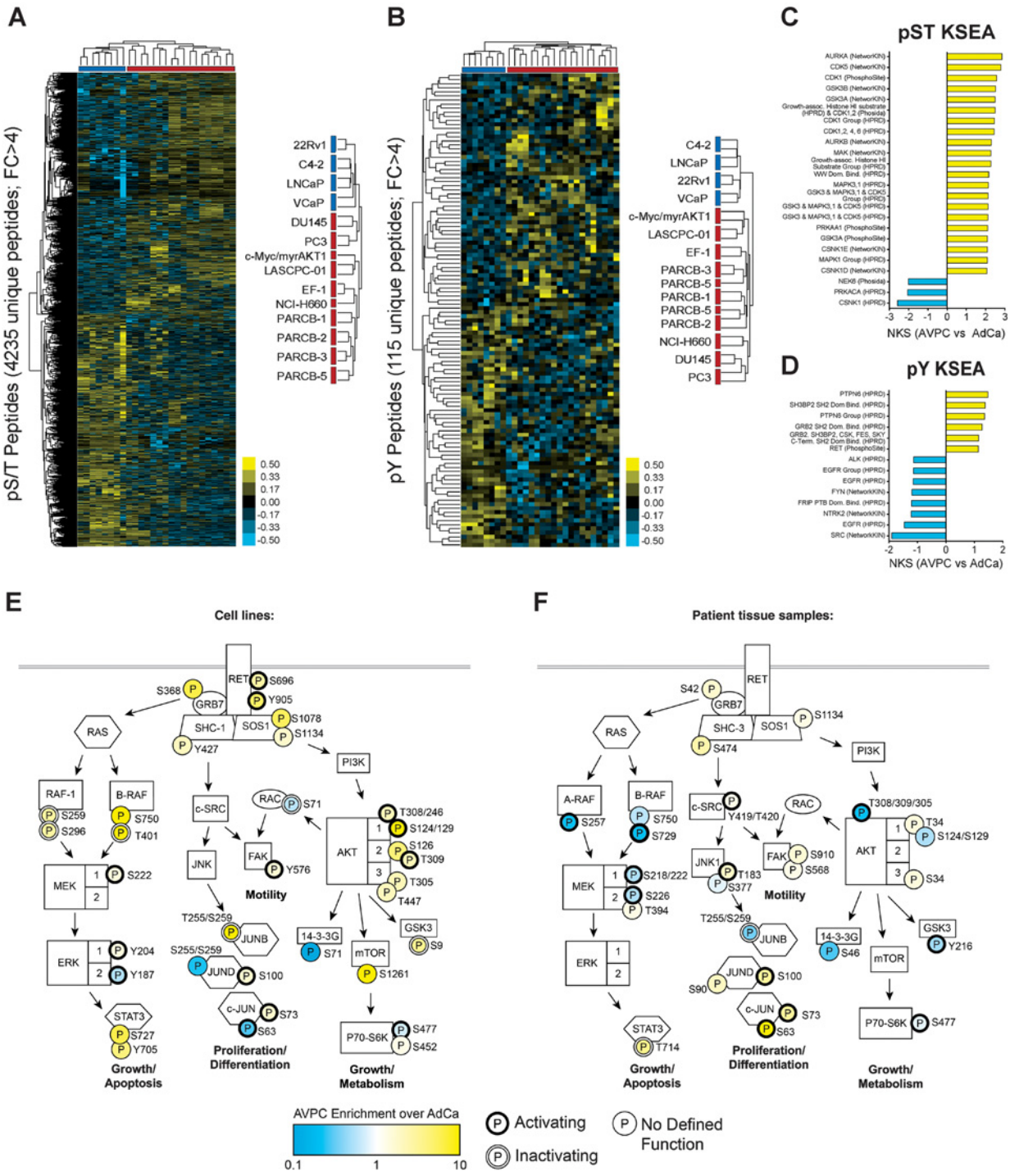

Figure 1.

Global phosphorylation and kinase signaling pathways are differentially regulated in AVPC cell lines compared with adenocarcinoma cell lines. Supervised hierarchical clustering heatmap of 4,235 unique phosphoserine/threonine (pS/T) enriched peptides (**A**) and 115 unique phosphotyrosine (pY) enriched peptides (**B**) from adenocarcinoma cell lines (blue: C4-2, 22Rv1, LNCaP, and VCaP) and AVPC cell lines (red: cMyc/myrAKT, LASCPC-01, EF-1, PARCB-1, PARCB-2, PARCB-3, PARCB-5, NCI-H660, DU145, and PC3). Yellow, hyperphosphorylation; blue, hypophosphorylation. **C** and **D,** Kinase substrate enrichment analysis (KSEA) performed on the 10 AVPC and 4 adenocarcinoma cell lines in **A** and **B**, showed multiple predicted alterations to kinase signaling. **C,** KSEA for pS/T analysis used a false discovery rate (FDR) <0.05, substrate hits > 5, and normalized K score >2.0. **D,** KSEA for pY analysis used an FDR < 0.1, substrate hits > 4, and normalized K score >1.1. **E,** Phosphorylated residues identified in the global phosphoproteomics from **A** and **B** or **F**. human phosphoproteome data (23) were mapped onto signaling pathways downstream of RET kinase. Yellow, enriched in AVPC relative to adenocarcinoma; blue, reduced in AVPC relative to adenocarcinoma. Thick black outline, activating phosphorylation; white outline, inactivating phosphorylation; thin outline, no defined function.

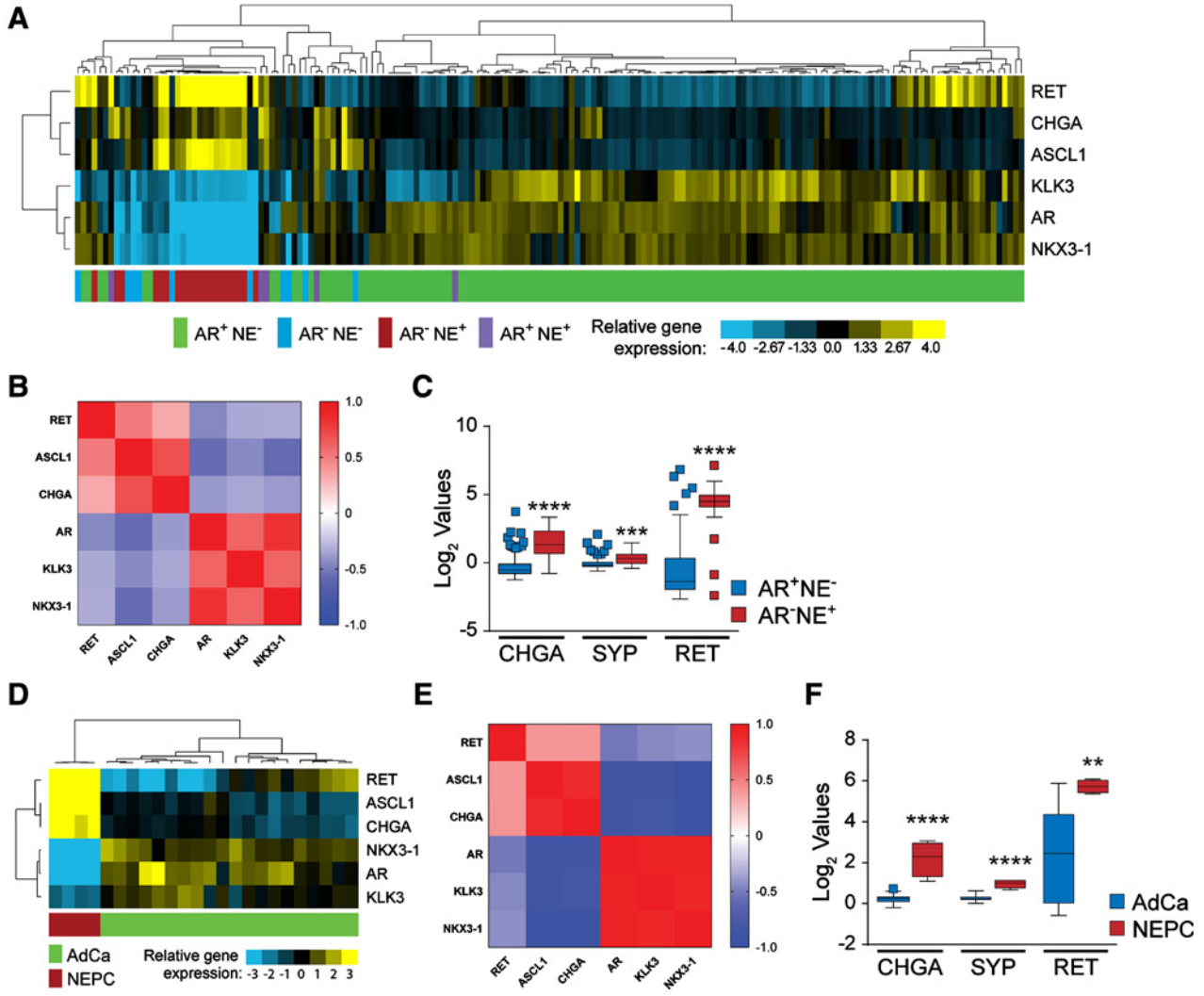

Figure 2.

RET kinase along with other neuroendocrine transcripts are upregulated in NEPC relative to adenocarcinoma patient samples. **A,** Microarray data from the University of Washington rapid autopsy data of metastatic prostate cancer biopsies (32) were clustered on the basis of gene expression of RET, neuroendocrine markers: CHGA and ASCL1, as well as androgen-regulated genes: KLK3, AR, and NKX3-1. Upregulation of expression is represented by yellow, while downregulated genes are represented by blue. Patient samples were classified by AR and NE markers as AR+NE- (green, $n = 134$), AR-NE- (blue, $n = 10$), AR-NE+ (red, $n = 20$), and AR+NE+ (purple, $n = 7$). **B,** Pearson correlation matrix of gene expression from **A** showing a correlation of RET gene expression with neuroendocrine markers and negative correlation with AR-responsive markers. **C,** Box and whisker plot of average transcript measurements of CHGA, SYP, or RET in adenocarcinoma (AR+NE-) versus the NEPC (AR-NE+) patients. The data is represented in Tukey plots and expression values were analyzed by Student *t* test. **D,** Agilent oligo array expression analysis of four neuroendocrine AR-negative LuCaP patient derived xenografts (PDX) and 20 LuCaP adenocarcinoma PDX published by Zhang and colleagues (33) were clustered as in **A**. **E,** Pearson correlation matrix of expression data represented in **D. F,** Box and whisker plot shows an upregulation in CHGA, SYP, and RET kinase in NEPC versus adenocarcinoma PDX samples. Data is represented as in **C**.

AR. AR expectedly showed strong correlation with AR regulators (CTNNB1, NCOA1 and CREBBP). To determine whether RET expression was required for cellular proliferation or viability, we compared the Project Achilles DEMETER scores of RET, highlighting the prostate cancer cell lines (**Fig. 3B**; ref. 29). The DEMETER score indicates how gene suppression affects cell viability compared with all other cell lines upon suppression of the same target gene. Among the seven prostate cancer cell lines, two of the AR independent AVPC cells, PC3 and NCI-H660, exhibited greater relative dependency on RET compared the 501 other cell lines (ranked 10th and 76th; Supplementary Table S8). This indicates RET kinase is required for the growth some AR-independent prostate cancer cell lines and not in the AR-dependent lines.

We validated the findings from the high-throughput short hairpin RNA (shRNA) screening by generating stable RET knockdown cell lines. The two most RET dependent cell lines from the large-scale screen, PC3 and NCI-H660, were stably transduced with two unique anti-RET shRNA constructs and the downregulation of RET protein or mRNA expression were confirmed (**Fig. 3C**; Supplementary Fig. S3A). RET knockdown strongly suppressed the growth of NCI-H660 cells, and to a lesser extent the PC3 cells. Interestingly, this correlates with the relative level of RET protein expression by Western blot analysis,

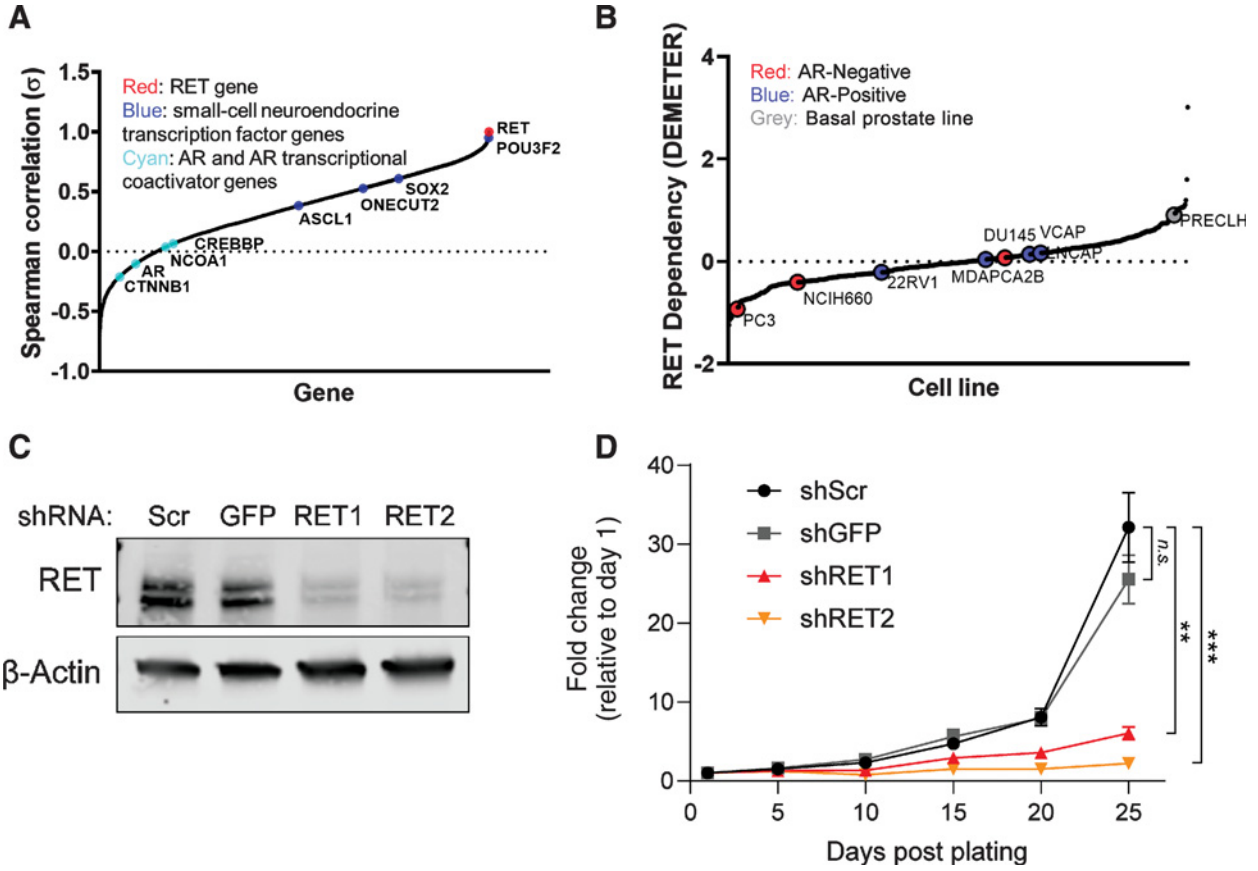

Figure 3.

RET expression correlates with NE markers in prostate cancer cell lines and is important for NEPC cell line growth. **A,** RET expression dependency profiling for 11,280 genes across eight prostate cell lines (PRECLH, LNCaP, VCaP, DU145, MDA PCa 2b, 22Rv1, NCI-H660, and PC3). RET expression was positively correlated with NEPC driver genes (blue) and negatively correlated with AR and AR regulators (cyan). **B,** Relative RET dependency scores reflect the ability of 503 cancer cell lines to maintain proliferation after RET knockdown (taken from the Project Achilles 2.201). Among the eight prostate cancer cell lines, PC3 and NCI-H660 cells showed the greatest dependency on RET. **C,** RET protein expression in NCI-H660 cells stably transduced with scrambled (Scr), anti-GFP, or two unique anti-RET shRNA. RET protein levels were reduced in two RET knockdown NCI-H660 cell lines and β-actin serves as a loading control. **D,** RET knockdown reduces cellular proliferation in H660 cell lines. The line graph represents relative cellular proliferation as measured by WST assay of one biological replicate. Cell proliferation was analyzed by linear regression of log-transformed data to determine statistical significance and error bars represent the SD of five technical replicates.

which is readily detectible in NCI-H660 cells and much lower in the PC3 cells (Supplementary Fig. S1). After 25 days of incubation, the total number of NCI-H660 cells decreased by 81% (shRET1, $P = 0.00013$) and 93% (shRET2, $P = 8.82 \times 10^{-5}$) compared with the scrambled shRNA (shScr) cells (**Fig. 3D**). The number of stable RET knockdown PC3 cells was 45% (shRET1, $P = 0.0021$) and 50% (shRET2, $P = 0.0021$) lower compared with shScr cells at day 8 (Supplementary Fig. S3B). Taken together, this suggests that RET kinase plays a role in enhancing NEPC cell growth and can be an effective therapeutic target for NEPC treatment.

RET kinase inhibitors block RET signaling in NEPC cells

AD80 is a novel, more selective inhibitor of the RET pathway than previous multityrosine kinase inhibitors such as cabozantinib or vandetanib (14, 15). However, AD80 still targets multiple other cellular kinases such as p70S6K, SRC, and VEGF receptors (15). We also utilized the newer RET inhibitors, LOXO-292 and BLU-667, which are currently undergoing clinical trials in RET fusion driven solid tumors and are considered specific RET inhibitors with few adverse effects (12, 13). To determine whether prostate cancer cells are sensitive to RET inhibition, we determined the IC_{50} of AD80, LOXO-292, BLU-667 in our panel of prostate cancer cell lines (Supplementary Fig. S4A). AD80 was consistently among the most effective at reducing viability, and the NCI-H660 cells were the most sensitive to AD80 of the RET inhibitors tested (Supplementary Figs. S4A–S4C). To confirm that RET kinase is active and can be inhibited by these drugs, we treated NCI-H660 cells with AD80, LOXO-292, BLU-667, or DMSO for 4 hours and evaluated the tyrosine phosphorylation of RET (37). RET kinase immunoprecipitated from RET inhibitor–treated NCI-H660 cells showed a reduction in total tyrosine phosphorylation, indicating that AD80, LOXO-292, and BLU-667 all inhibit the activation of RET in NCI-H660 cells (**Fig. 4A**). Next, we measured the downstream targets of RET by looking at phosphorylation of ERK1/2 and AKT1/2. Interestingly, all three drugs reduced ERK1/2 phosphorylation of residues Tyr202/Try204 in a dose-dependent manner, but AD80 was the most effective in reducing phosphorylation of both ERK1/2 and AKT1/2, while having no effect on the total protein levels (**Fig. 4B**). Cabozantinib and vandetanib also decreased the levels of phospho ERK1/2 and AKT1/2 in NCI-H660 cells (Supplementary Fig. S4D). Finally, we treated the RET

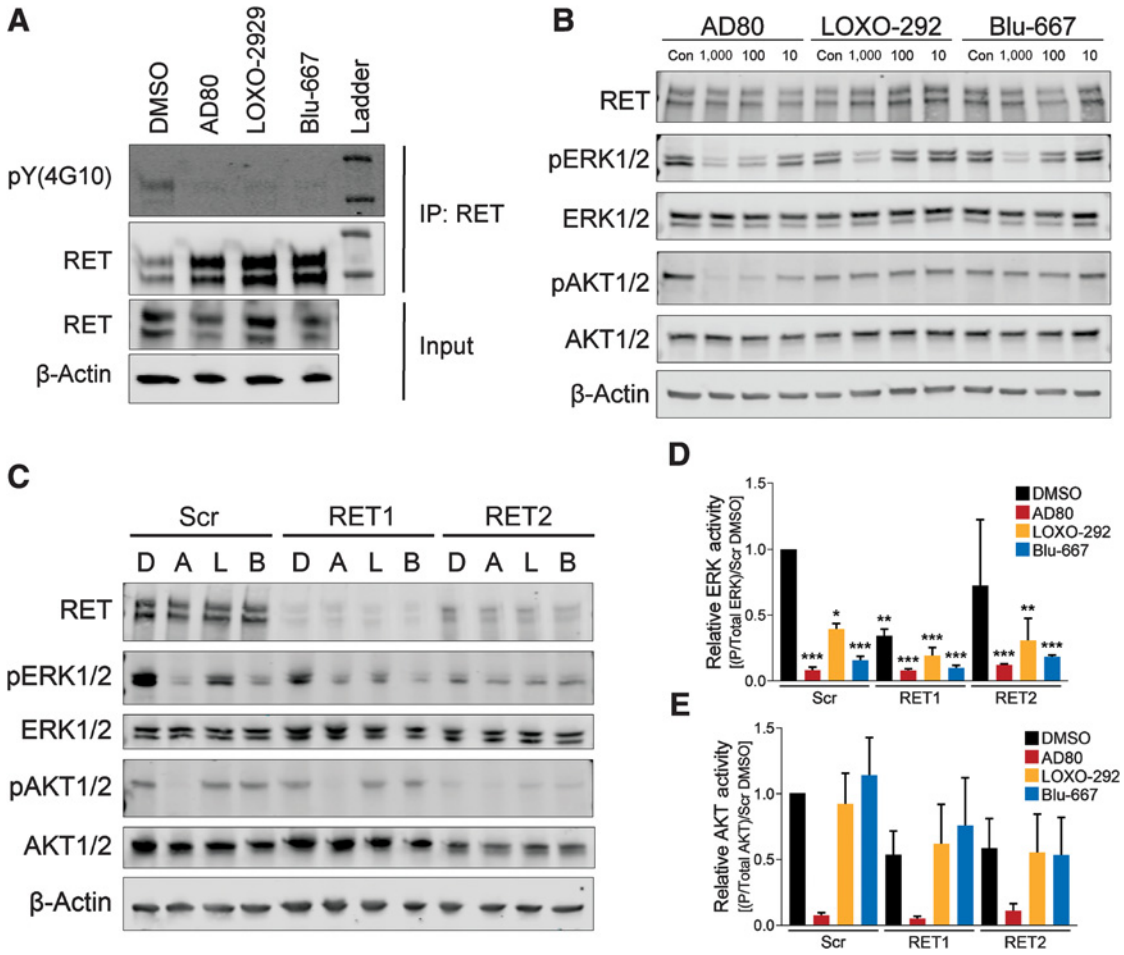

Figure 4.

NCI-H660 cells are sensitive to RET inhibition and show sensitivity to RET inhibitors. **A,** Immunoprecipitation of RET kinase from H660 cells shows that 4-hour treatment with 1 μmol/L AD80, LOXO-292, or BLU-667 reduces RET tyrosine phosphorylation, as assayed with a total phosphotyrosine antibody 4G10. **B,** NCI-H660 cells treated for 4 hours with DMSO (Con) the indicated concentrations (nmol/L) of AD80, LOXO-292, or BLU-667, showed reduced activity of the MAPK and AKT signaling cascades downstream of RET. Activity was analyzed by Western blot analysis for phosphorylation of ERK1/2 at Tyr202/Tyr204 and phosphorylation of AKT1/2 at Ser473. The AD80 treatment reduced phosphorylation of both downstream targets, while LOXO-292 and BLU-667 reduced the activity of ERK1/2. In all treatments the total ERK1/2, total AKT1/2, and actin loading control remained unaffected. **C,** The activity of pERK1/2 (Tyr202/Tyr204) and pAKT1/2 (Ser 473) in NCI-H660 scrambled control and RET knockdown cells was assayed after a 4-hour treatment with DMSO (D), or 1 μmol/L of AD80 (A), LOXO-292 (L), or BLU-667 (B). **D,** The relative ERK1/2 activity was measured by comparing pERK1/2 (Tyr202/Tyr204) to total ERK1/2 protein and normalized to the scrambled DMSO-treated sample. The ERK1/2 activity is reduced by both RET knockdown and after treatment with RET inhibitors. The bars represent the average values from three experiments and the error bars are SD. **E,** Quantification of AKT1/2 activity (pAKT1/2 S473 relative to total AKT protein and normalized DMSO-treated Scr cells) shows AD80 potently inhibits AKT1/2 activity while knockdown may reduce activity slightly. Bars represent the mean from three experiments and the error bars are SD.

knockdown cells with AD80, LOXO-292, or BLU-667 (**Fig. 4C**). We found that RET knockdown reduced the levels of ERK1/2 phosphorylation and to a lesser extent AKT1/2 (**Fig. 4D** and **E**). The effect of AD80, LOXO-292, and BLU-667 was reduced in the RET knockdown cells, suggesting that RET is required for full activation of ERK1/2 and AKT1/2 (**Fig. 4D** and **E**). The ability of these RET inhibitors to reduce viability (IC_{50}) combined with genetic knockdown of RET in NCI-H660 cells (**Fig. 3**) suggests that RET kinase is critical to the growth and survival of NEPC cells with high RET expression and can be pharmacologically inhibited.

RET inhibition induces cell death in NEPC 3D culture models

We cultured NCI-H660 cells as 3D spheroids and tested the ability of AD80 to induce cell death (Supplementary Fig. S4E). The calculated LD_{50} for the NCI-H660 organoids was 1.4 μmol/L, slightly higher than cells in 2D culture. The organoids clearly displayed an increase in dead cells at higher doses of AD80 (Supplementary Fig. S4F). We extended our RET inhibitor treatment studies to a second organoid model of NEPC (5). Tumors derived from the prostate epithelium of $Pten^{-/-}Rb^{-/-}$ (DKO) mice express higher levels of RET mRNA than $Pten^{-/-}$ (SKO) or wild-type (WT) animals (Supplementary Fig. S5A; ref. 5). Immunofluorescence staining also confirmed an increase of RET kinase protein in the DKO organoids and low to absent RET kinase in the SKO organoids (Supplementary Fig. S5B). The DKO organoids were also resistant to enzalutamide treatment, mimicking the ADT-resistant characteristic of NEPC prostate cancer cells that express high levels of RET (Supplementary Fig. S5C). Treating the

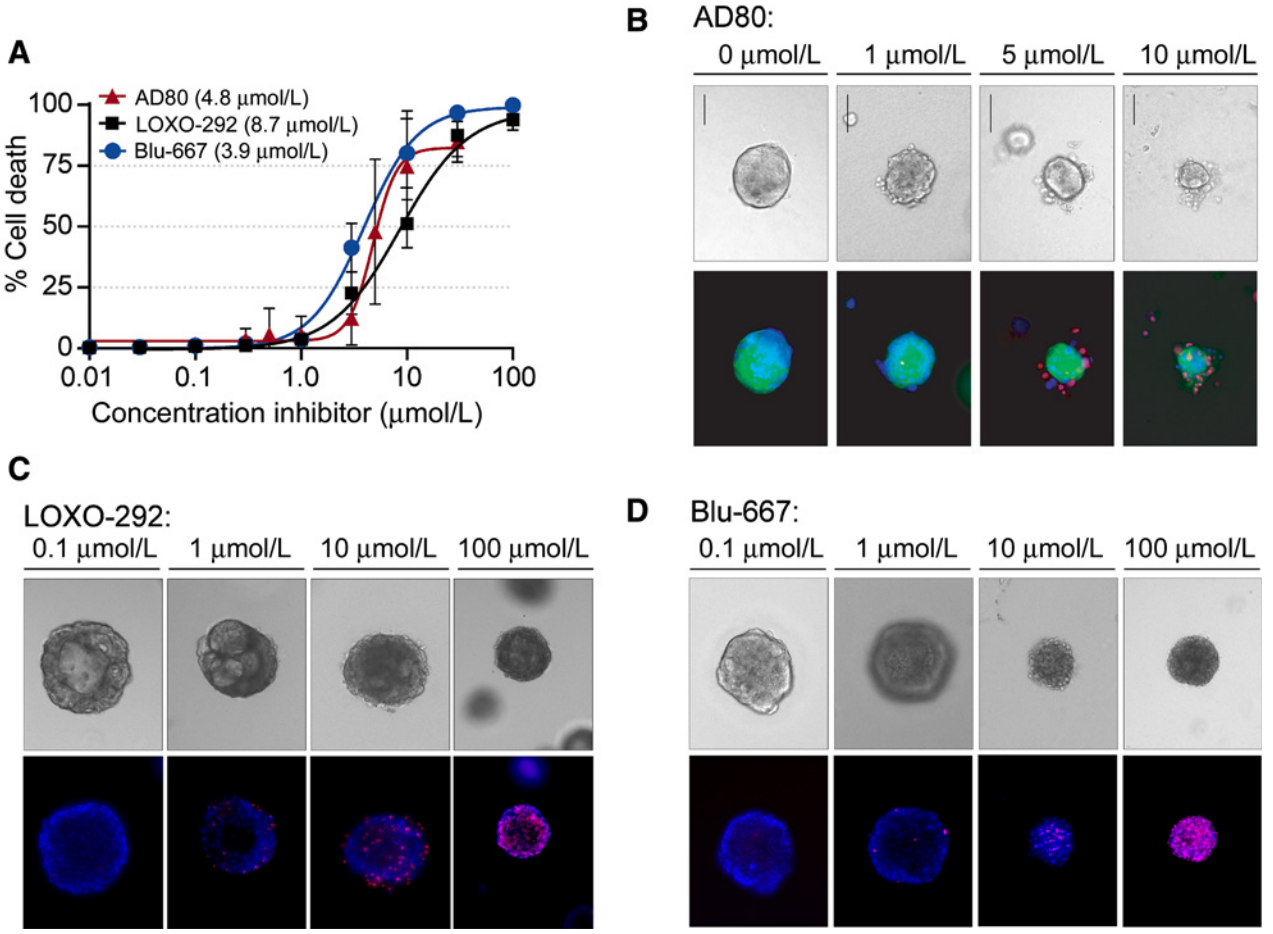

Figure 5.

Organoid NEPC models are sensitive to treatment with multiple RET inhibitors. **A,** A dose–response curve of Pten$^{-/-}$ and Rb$^{-/-}$ prostate specific double knockout (DKO) organoids treated with increasing concentrations of AD80, LOXO-292, and BLU-667. Viability was measured by staining for dead cells. Circles represent mean and error bars ± SD. **B,** Bright field images and corresponding fluorescence images of GFP-labeled DKO organoids treated with the indicated concentrations of AD80. Blue, DAPI staining of nuclei; red, propidium iodide staining of dead cells. Scale bar, 100 μm. Representative brightfield and fluorescent images of LOXO-292 (**C**) and BLU-667 (**D**) DKO organoids treated with the indicated concentrations of drugs stained as described in **E** with the GFP channel omitted.

DKO organoids with increasing concentrations of AD80, LOXO-292, or BLU-667 induced a dose-dependent increase in cell death, as assayed by live-dead PI staining of the organoids (**Fig. 5A–D**). All three drugs displayed a similar LD_{50}, suggesting that RET inhibition is effective in preventing tumor growth in a second model of NEPC.

AD80 reduces growth of NEPC xenograft tumors *in vivo* by increasing cell death

To test the efficacy of AD80 in an *in vivo* model system of NEPC, we generated NCI-H660 xenograft tumors in NOD-SCID mice. Once tumors reached 100–200 mm^3, mice were randomized and placed into one of two treatment groups: Control (DMSO) or 10 mg/kg AD80 (**Fig. 6A**). Over the course of the 22-day treatment, AD80-treated tumors showed a significant reduction in overall tumor volume (**Fig. 6B**) without a significant effect on animal weight (**Fig. 6C**). This experiment was repeated in a second cohort of mice with 24 days of treatment and higher dose of AD80 (20 mg/kg; Supplementary Fig. S6). The higher dose of AD80 was associated with increased toxicity, but showed similar inhibition of tumor growth throughout the 24-day treatment (Supplementary Fig. S6A–S6C). To interrogate the molecular characteristics of AD80 treatment, the tumors (**Fig. 6D**) were fixed and sectioned for staining. Sections stained with hematoxylin & eosin (H&E) showed similar tumor morphology (**Fig. 6E**; Supplementary Fig. S6D). IHC staining for RET showed similar expression and localization among the treatment groups (**Fig. 6E** and **F**; Supplementary Figs. S6D and S6E). There was also no difference in tumor proliferation as assayed by Ki67 staining among the treatment groups in either cohort of mice (**Fig. 6E** and **G**; Supplementary Figs. S6D and S6F). However, TUNEL staining showed large regions of positive staining and the percentage of total tumor area that stained positive trended higher in the AD80-treated groups (**Fig. 6E** and **H**; Supplementary Fig. S6D and S6G). Taken together, these results suggest that AD80 treatment is effective in limiting tumor growth by inducing cell death in neuroendocrine cells with high RET expression and that the specific population of patients that have high RET expression, are refractory to ADT, and have few remaining therapeutic options may benefit from RET kinase inhibitor therapies.

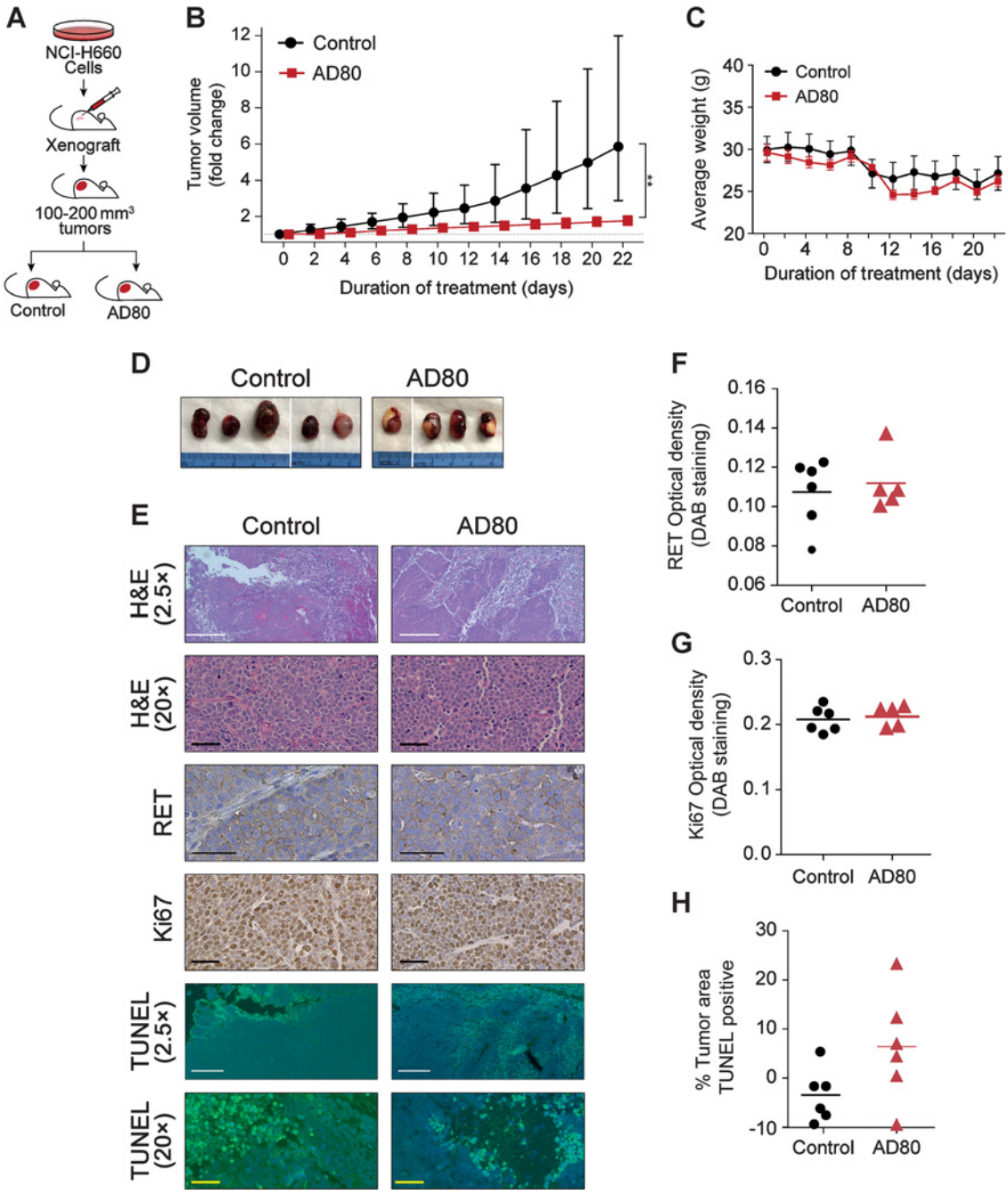

Figure 6.

AD80 reduces NCI-H660 xenograft tumor growth. **A,** Schematic of *in vivo* study in which NCI-H660 cells were injected subcutaneously into the right flank of NOD-SCID mice and tumors were allowed to grow to approximately 100 to 200 mm^3 before being randomly assigned into two treatment groups: control (DMSO alone, $n = 6$) or AD80 (10 mg/kg/day, $n = 6$). **B,** The fold change in tumor volume by treatment group was plotted as a function of the number of days of treatment. Means and CIs were calculated on the log scale and reported in terms of geometric means after exponentiation with error bars ± 95% CI. There was evidence of an overall treatment effect on tumor growth rate ($P = 0.006$) with a significantly lower tumor volume at day 22 ($P = 0.006$). **C,** Average animal weights were measured at the same time as tumor volumes and no differences in average animal weight between treatment groups was observed over the duration of the study. Symbols represent means with error bars ± SE. **D,** Following the termination of the xenograft tumor experiment, tumors were excised from animals that survived to the end of the study and photographed with a centimeter scale ruler. Separate images from the same group are divided by a white line. **E,** Representative images of H&E (2.5× and 20×), RET IHC (20×), Ki67 IHC (20×), and TUNEL (2.5× and 20×) stained sections of tumors from each group. White scale bars, 500 μm. Yellow and black scale bars, 50 μm. Average optical density of RET staining (**F**) and Ki67 staining (**G**) from five distinct fields of view in each tumor are represented by symbols with a horizontal bar representing the mean. Quantification was analyzed by one way ANOVA. **H,** Quantification of the average TUNEL positive area (2.5×) was analyzed with the Kruskal–Wallis test ($P = 0.1727$). Symbols represent averages for individual tumors with a horizontal line representing the mean. Bars represent the mean with error bars represent ± SE.

Discussion

Increasing evidence points to the activation of kinase pathways as possible key mechanisms that bypass AR-targeted therapies and allow the tumors to continue to survive such a harsh therapeutic environment (1, 4, 20, 23). Utilizing phosphoproteomics, we showed that AR-independent cell lines have altered kinase signaling pathways compared with AR-driven adenocarcinomas, which includes activation of RET kinase. Multiple proteins downstream of the RET kinase pathway were phosphorylated on activating residues in both the cell line and in mCRPC autopsy patient samples. RET mutations or activating rearrangements are drivers of tumor development and growth in MEN2, medullary thyroid cancer, and small-cell and non–small cell lung cancers, and drugs targeting RET can extend survival of these patients (38–40). Cabozantinib, which inhibits RET kinase and other receptor tyrosine kinases including VEGR1/2, has extended survival in certain cancers with activating RET mutations (41, 42). In prostate cancer, cabozantinib showed promise in phase II clinical trials but failed to meet the endpoint criteria in phase III trials (NCT01605227) (43, 44). However, this was tested in a nonstratified patient population and did not focus on NEPC or patients with high RET expression (45). A retrospective evaluation of postdocetaxel patients with CRPC in the COMET-1 and COMET-2 phase III clinical trials where cabozantinib was compared with prednisone and prednisone plus mitoxantrone suggest a subpopulation exists that may benefit from cabozantinib treatment, highlighting the importance of molecular stratification of patients for individualized treatments (43, 44, 46). Recently, RET knockdown in a prostate AdCa cell line, LNCaP, was reported to restrict tumor growth, but it remains unclear if and how RET contributes to tumor progression in NEPC (11).

We found that overall RET expression in prostate cancer patient samples is highly variable, but that RET kinase expression correlated very strongly with NEPC. In the datasets we analyzed, there were examples of metastatic and treatment induced NEPC tumors (based on molecular and pathologic features) that lacked RET gene expression. Inversely, there were also patients classified as AR-positive adenocarcinomas that displayed high levels of RET gene expression but lacked expression of other neuroendocrine lineage markers (**Fig. 2**; Supplementary Fig. S2). It is important to note that the transition from adenocarcinoma to NEPC may be dynamic (5) and RET expression in AR-positive tumors may suggest that these tumors are either a heterogeneous phenotype or are transitioning from adenocarcinoma to NEPC. Currently, little is known about the regulation of RET gene expression in prostate cancer. Several key epigenetic regulators (such as CBX2, EZH2, BRN2, and SOX2) have been identified as possible modulators that can switch tumors between an adenocarcinoma and NEPC state (5, 47–49). We found that RET kinase dependency correlated with several of these transcription factors (**Fig. 3**). Alterations in DNA methylation or transcriptional regulation resulting from the loss of proteins such as RB1 may further alter RET expression and activity. Therefore, it remains to be determined how robust RET expression is gained during the transition from mCRPC to a NEPC phenotype. In small-cell lung cancer, ASCL1 was shown to induce RET gene expression and this mechanism of regulation may hold true in NEPC, but has not been validated (50).

Regardless of the dynamics of RET expression in disease progression, we showed that multiple RET kinase pathway inhibitors effectively restricted growth in the *Rb/Pten* knockout organoids and AD80 reduced the growth of the NCI-H660 cell line and spheroids *in vitro*, as well as NCI-H660 tumors *in vivo*. We validated our inhibitor studies by knocking down RET in NCI-H660 and PC3 cell lines and saw a similar reduction in overall growth. The pharmacologic and genetic inhibition of RET kinase suggests that RET kinase signaling is important for NEPC tumor progression. To identify patients that could benefit from treatment including RET inhibition, it will be important to generate assays or validate markers of RET activity in NEPC. Pathology, loss of AR signaling, or expression of neuroendocrine genes are not sufficient alone to identify all patients with high levels of RET expression that may benefit from RET-targeted therapies. Moving forward, it will be important to identify the subset of patients that would benefit from inhibition of RET kinase. Development of biomarkers for transcriptional activators, RET protein, or markers of RET activity will enable pre-selection of individuals who would benefit from RET inhibitors. Understanding the regulation of RET gene expression, correlation of RET expression and activity and disease progression, as well as the contribution of RET kinase to mCRPC tumor progression could inform better treatment strategies.

Disclosure of Potential Conflicts of Interest

O.N. Witte reports personal fees and other from Allogene Therapeutics, other from Kronos Bio, other from Trethera, other from Sofie Biosciences, other from Breakthrough Properties, other from Nammi Therapeutics, and personal fees and other from Vida Ventures during the conduct of the study. P.S. Nelson reports personal fees from Astellas, personal fees from Janssen, and personal fees from Bristol Myers Squibb outside the submitted work. No potential conflicts of interest were disclosed by the other authors.

Disclaimer

The content is solely the responsibility of the authors and does not necessarily represent the official views of the NIH.

Authors' Contributions

H.R. VanDeusen: Conceptualization, data curation, formal analysis, validation, investigation, methodology, writing-original draft, writing-review and editing. **J.R. Ramroop:** Conceptualization, data curation, formal analysis, validation, investigation, methodology, writing-original draft, writing-review and editing. **K.L. Morel:** Data curation, formal analysis, investigation, writing-review and editing. **S.Y. Bae:** Data curation, formal analysis, investigation, methodology, writing-review and editing. **A.V. Sheahan:** Data curation. **Z. Sychev:** Formal analysis, methodology. **N.A. Lau:** Data curation, investigation. **L.C. Cheng:** Data curation, formal analysis, investigation. **V.M. Tan:** Data curation, investigation. **Z. Li:** Data curation, formal analysis, investigation, methodology. **A. Petersen:** Software, formal analysis, methodology, writing-review and editing. **J.K. Lee:** Data curation, supervision, investigation, writing-review and editing. **J.W. Park:** Resources, resources. **R. Yang:** Resources, formal analysis. **J.H. Hwang:** Formal analysis, investigation, visualization, methodology, writing-review and editing. **I. Coleman:** Resources. **O.N. Witte:** Resources, supervision, investigation, writing-review and editing. **C. Morrissey:** Resources, data curation, supervision, writing-review and editing. **E. Corey:** Resources, data curation, supervision, writing-review and editing. **P.S. Nelson:** Resources, data curation, supervision, writing-review and editing. **L. Ellis:** Conceptualization, data curation, formal analysis, supervision, funding acquisition, investigation, visualization, methodology, writing-review and editing. **J.M. Drake:** Conceptualization, resources, data curation, formal analysis, supervision, funding acquisition, validation, investigation, visualization, methodology, writing-original draft, project administration, writing-review and editing.

Acknowledgments

We thank members of the Drake lab for providing advice and input on the manuscript. We also thank the members of the Biological Mass Spectrometry Facility of Robert Wood Johnson Medical School and Rutgers, The State University of New Jersey, for providing advice and performing mass spectrometry on our samples. We thank Ryder Clifford from QGel for providing reagents. We thank the patients and their families, Celestia Higano, Evan Yu, Elahe Mostaghel, Heather Cheng, Bruce Montgomery, Mike Schweizer, Andrew Hsieh, Daniel Lin, Funda Vakar-Lopez, Lawrence True and the rapid autopsy teams for their contributions to the University of Washington Medical Center Prostate Cancer Donor Rapid Autopsy Program and

the Development of the LuCaP PDX models. H.R. VanDeusen is supported by Department of Defense Prostate Cancer Research Program W81XWH-19-1-0173. This work was also supported by the Department of Defense grant (W81XWH-17-1-0414; W81XWH-17-1-0415; W81XWH-18-1-0347), the Prostate Cancer Biorepository Network (PCBN; W81XWH-14-2-0183), the Pacific Northwest Prostate Cancer SPORE (P50CA97186), the PO1 NIH grant (PO1 CA163227), the Richard M. LUCAS Foundation, and the Institute for Prostate Cancer Research (IPCR). L.C. Cheng and V.M. Tan are supported by the National Institute of General Medical Sciences of the NIH under award number T32 GM008339. J.W. Park is supported by the NIH/NCI grant K99/R00 Pathway to Independence award K99CA218731/R00CA218731. R. Yang is supported by Department of Defense Prostate Cancer Research Program W81XWH-19-1-0161. J.H. Hwang is supported by American Cancer Society-AstraZeneca (PF-16-142-01-TBE). O.N. Witte is supported by the Zimmerman Family, the Concern Foundation, and by a Prostate Cancer Foundation Challenge Award. O.N. Witte is also supported by the West Coast Prostate Cancer Dream Team supported by a Stand Up to Cancer-Prostate Cancer Foundation-Prostate Cancer Dream Team Translational Cancer Research Grant (SU2C-AACR-DT0812; co-principal investigator: O.N. Witte). This research grant is made possible by the generous support of the Movember Foundation. Stand Up To Cancer is a division of the Entertainment Industry Foundation. The research grant is administered by the American Association for Cancer Research. L. Ellis is supported by the Department of Defense Prostate Cancer Research Program W81XWH-18-1-0541. J. M. Drake is supported by the Department of Defense Prostate Cancer Research Program W81XWH-14-1-0148, W81XWH-15-1-0236 and W81XWH-18-1-0542, Prostate Cancer Foundation Young Investigator Award, and the New Jersey Health Foundation. Research reported in this publication was also supported by the National Center for Advancing Translational Sciences of the National Institutes of Health Award Number UL1-TR002494.

The costs of publication of this article were defrayed in part by the payment of page charges. This article must therefore be hereby marked *advertisement* in accordance with 18 U.S.C. Section 1734 solely to indicate this fact.

Received December 23, 2019; revised April 1, 2020; accepted May 19, 2020; published first May 27, 2020.

References

1. Bluemn EG, Coleman IM, Lucas JM, Coleman RT, Hernandez-Lopez S, Tharakan R, et al. Androgen receptor pathway-independent prostate cancer is sustained through FGF signaling. Cancer Cell 2017;32:474–89.
2. Beltran H, Tomlins S, Aparicio A, Arora V, Rickman D, Ayala G, et al. Aggressive variants of castration-resistant prostate cancer. Clin Cancer Res 2014;20:2846–50.
3. Aparicio AM, Harzstark AL, Corn PG, Wen S, Araujo JC, Tu SM, et al. Platinum-based chemotherapy for variant castrate-resistant prostate cancer. Clin Cancer Res 2013;19:3621–30.
4. Beltran H, Oromendia C, Danila DC, Montgomery B, Hoimes C, Szmulewitz RZ, et al. A phase II trial of the aurora kinase a inhibitor alisertib for patients with castration-resistant and neuroendocrine prostate cancer: efficacy and biomarkers. Clin Cancer Res 2019;25:43–51.
5. Ku SY, Rosario S, Wang Y, Mu P, Seshadri M, Goodrich ZW, et al. Rb1 and Trp53 cooperate to suppress prostate cancer lineage plasticity, metastasis, and antiandrogen resistance. Science 2017;355:78–83.
6. Beltran H, Rickman DS, Park K, Chae SS, Sboner A, MacDonald TY, et al. Molecular characterization of neuroendocrine prostate cancer and identification of new drug targets. Cancer Discov 2011;1:487–95.
7. Blume-Jensen P, Hunter T. Oncogenic kinase signalling. Nature 2001;411:355–65.
8. Arighi E, Borrello MG, Sariola H. RET tyrosine kinase signaling in development and cancer. Cytokine Growth Factor Rev 2005;16:441–67.
9. Drake JM, Graham NA, Lee JK, Stoyanova T, Faltermeier CM, Sud S, et al. Metastatic castration-resistant prostate cancer reveals intrapatient similarity and interpatient heterogeneity of therapeutic kinase targets. Proc Natl Acad Sci U S A 2013;110:E4762–9.
10. Lee JK, Bangayan NJ, Chai T, Smith BA, Pariva TE, Yun S, et al. Systemic surfaceome profiling identifies target antigens for immune-based therapy in subtypes of advanced prostate cancer. Proc Natl Acad Sci U S A 2018;115:E4473–82.
11. Ban K, Feng S, Shao L, Ittmann M. RET signaling in prostate cancer. Clin Cancer Res 2017;23:4885–96.
12. Subbiah V, Gainor JF, Rahal R, Brubaker JD, Kim JL, Maynard M, et al. Precision targeted therapy with BLU-667 for RET-driven cancers. Cancer Discov 2018;8:836–49.
13. Subbiah V, Velcheti V, Tuch BB, Ebata K, Busaidy NL, Cabanillas ME, et al. Selective RET kinase inhibition for patients with RET-altered cancers. Ann Oncol 2018;29:1869–76.
14. Plenker D, Riedel M, Bragelmann J, Dammert MA, Chauhan R, Knowles PP, et al. Drugging the catalytically inactive state of RET kinase in RET-rearranged tumors. Sci Transl Med 2017;9:eaah6144.
15. Dar AC, Das TK, Shokat KM, Cagan RL. Chemical genetic discovery of targets and anti-targets for cancer polypharmacology. Nature 2012;486:80–4.
16. Cheng LC, Li Z, Graeber TG, Graham NA, Drake JM. Phosphopeptide enrichment coupled with label-free quantitative mass spectrometry to investigate the phosphoproteome in prostate cancer. J Vis Exp 2018;138:e57996.
17. Scheltema RA, Hauschild JP, Lange O, Hornburg D, Denisov E, Damoc E, et al. The Q exactive HF, a Benchtop mass spectrometer with a pre-filter, high-performance quadrupole and an ultra-high-field Orbitrap analyzer. Mol Cell Proteomics 2014;13:3698–708.
18. Cox J, Mann M. MaxQuant enables high peptide identification rates, individualized p.p.b.-range mass accuracies and proteome-wide protein quantification. Nat Biotechnol 2008;26:1367–72.
19. Vizcaino JA, Cote RG, Csordas A, Dianes JA, Fabregat A, Foster JM, et al. The PRoteomics IDEntifications (PRIDE) database and associated tools: status in 2013. Nucleic Acids Res 2013;41:D1063–9.
20. Drake JM, Paull EO, Graham NA, Lee JK, Smith BA, Titz B, et al. Phosphoproteome integration reveals patient-specific networks in prostate cancer. Cell 2016;166:1041–54.
21. Eisen MB, Spellman PT, Brown PO, Botstein D. Cluster analysis and display of genome-wide expression patterns. Proc Natl Acad Sci U S A 1998;95:14863–8.
22. Saldanha AJ. Java Treeview–extensible visualization of microarray data. Bioinformatics 2004;20:3246–8.
23. Drake JM, Graham NA, Stoyanova T, Sedghi A, Goldstein AS, Cai H, et al. Oncogene-specific activation of tyrosine kinase networks during prostate cancer progression. Proc Natl Acad Sci U S A 2012;109:1643–8.
24. Uphoff CC, Drexler HG. Detecting mycoplasma contamination in cell cultures by polymerase chain reaction. Methods Mol Biol 2011;731:93–103.
25. Stoyanova T, Cooper AR, Drake JM, Liu X, Armstrong AJ, Pienta KJ, et al. Prostate cancer originating in basal cells progresses to adenocarcinoma propagated by luminal-like cells. Proc Natl Acad Sci U S A 2013;110:20111–6.
26. Lee JK, Phillips JW, Smith BA, Park JW, Stoyanova T, McCaffrey EF, et al. N-Myc drives neuroendocrine prostate cancer initiated from human prostate epithelial cells. Cancer Cell 2016;29:536–47.
27. Park JW, Lee JK, Sheu KM, Wang L, Balanis NG, Nguyen K, et al. Reprogramming normal human epithelial tissues to a common, lethal neuroendocrine cancer lineage. Science 2018;362:91–5.
28. Drost J, Karthaus WR, Gao D, Driehuis E, Sawyers CL, Chen Y, et al. Organoid culture systems for prostate epithelial and cancer tissue. Nat Protoc 2016;11:347–58.
29. Tsherniak A, Vazquez F, Montgomery PG, Weir BA, Kryukov G, Cowley GS, et al. Defining a cancer dependency map. Cell 2017;170:564–76.
30. Cowley GS, Weir BA, Vazquez F, Tamayo P, Scott JA, Rusin S, et al. Parallel genome-scale loss of function screens in 216 cancer cell lines for the identification of context-specific genetic dependencies. Sci Data 2014;1:140035.
31. Schindelin J, Arganda-Carreras I, Frise E, Kaynig V, Longair M, Pietzsch T, et al. Fiji: an open-source platform for biological-image analysis. Nat Methods 2012;9:676–82.
32. Kumar A, Coleman I, Morrissey C, Zhang X, True LD, Gulati R, et al. Substantial interindividual and limited intraindividual genomic diversity among tumors from men with metastatic prostate cancer. Nat Med 2016;22:369–78.
33. Zhang X, Coleman IM, Brown LG, True LD, Kollath L, Lucas JM, et al. SRRM4 expression and the loss of REST activity may promote the emergence of the neuroendocrine phenotype in castration-resistant prostate cancer. Clin Cancer Res 2015;21:4698–708.
34. Abida W, Cyrta J, Heller G, Prandi D, Armenia J, Coleman I, et al. Genomic correlates of clinical outcome in advanced prostate cancer. Proc Natl Acad Sci U S A 2019;116:11428–36.

35. Aggarwal R, Huang J, Alumkal JJ, Zhang L, Feng FY, Thomas GV, et al. Clinical and genomic characterization of treatment-emergent small-cell neuroendocrine prostate cancer: a multi-institutional prospective study. J Clin Oncol 2018;36: 2492–503.
36. Beltran H, Prandi D, Mosquera JM, Benelli M, Puca L, Cyrta J, et al. Divergent clonal evolution of castration-resistant neuroendocrine prostate cancer. Nat Med 2016;22:298–305.
37. Mulligan LM. RET revisited: expanding the oncogenic portfolio. Nat Rev Cancer 2014;14:173–86.
38. Phay JE, Shah MH. Targeting RET receptor tyrosine kinase activation in cancer. Clin Cancer Res 2010;16:5936–41.
39. Donis-Keller H, Dou S, Chi D, Carlson KM, Toshima K, Lairmore TC, et al. Mutations in the RET proto-oncogene are associated with MEN 2A and FMTC. Hum Mol Genet 1993;2:851–6.
40. Dabir S, Babakoohi S, Kluge A, Morrow JJ, Kresak A, Yang M, et al. RET mutation and expression in small-cell lung cancer. J Thorac Oncol 2014;9:1316–23.
41. Ernani V, Kumar M, Chen AY, Owonikoko TK. Systemic treatment and management approaches for medullary thyroid cancer. Cancer Treat Rev 2016;50:89–98.
42. Gautschi O, Milia J, Filleron T, Wolf J, Carbone DP, Owen D, et al. Targeting RET in patients with RET-rearranged lung cancers: results from the global, multicenter RET registry. J Clin Oncol 2017;35:1403–10.
43. Smith M, De Bono J, Sternberg C, Le Moulec S, Oudard S, De Giorgi U, et al. Phase III study of cabozantinib in previously treated metastatic castration-resistant prostate cancer: COMET-1. J Clin Oncol 2016;34:3005–13.
44. Sonpavde GP, Pond GR, Fizazi K, de Bono JS, Basch EM, Scher HI, et al. Cabozantinib for progressive metastatic castration-resistant prostate cancer following docetaxel: combined analysis of two phase 3 trials. Eur Urol Oncol 2018 Nov 30 [Epub ahead of print].
45. Smith DC, Smith MR, Sweeney C, Elfiky AA, Logothetis C, Corn PG, et al. Cabozantinib in patients with advanced prostate cancer: results of a phase II randomized discontinuation trial. J Clin Oncol 2013;31:412–9.
46. Basch EM, Scholz M, de Bono JS, Vogelzang N, de Souza P, Marx G, et al. Cabozantinib versus mitoxantrone-prednisone in symptomatic metastatic castration-resistant prostate cancer: a randomized phase 3 trial with a primary pain endpoint. Eur Urol 2019;75:929–37.
47. Clermont PL, Lin D, Crea F, Wu R, Xue H, Wang Y, et al. Polycomb-mediated silencing in neuroendocrine prostate cancer. Clin Epigenetics 2015;7:40.
48. Bishop JL, Thaper D, Vahid S, Davies A, Ketola K, Kuruma H, et al. The master neural transcription factor BRN2 is an androgen receptor-suppressed driver of neuroendocrine differentiation in prostate cancer. Cancer Discov 2017;7:54–71.
49. Mu P, Zhang Z, Benelli M, Karthaus WR, Hoover E, Chen CC, et al. SOX2 promotes lineage plasticity and antiandrogen resistance in TP53- and RB1-deficient prostate cancer. Science 2017;355:84–8.
50. Kosari F, Ida CM, Aubry MC, Yang L, Kovtun IV, Klein JL, et al. ASCL1 and RET expression defines a clinically relevant subgroup of lung adenocarcinoma characterized by neuroendocrine differentiation. Oncogene 2014;33: 3776–83.